PATTERNS OF CLIMATE VARIABILITY IN THE WESTERN EQUATORIAL PACIFIC DURING THE COMMON ERA

By

KATHERINE LEE ESSWEIN

A thesis submitted to the

Graduate School of New Brunswick Rutgers,

The State University of New Jersey

in partial fulfillment of the requirements

for the degree of Master of Science

Graduate Program in Oceanography

written under the direction of

Yair Rosenthal

and approved by

____

____

____

New Brunswick, New Jersey

October, 2012

ABSTRACT OF THE THESIS

Patterns of climate variability in the Western Equatorial Pacific during the Common Era

By KATHERINE LEE ESSWEIN

Thesis Director:
Yair Rosenthal

Paleoclimate records suggest significant multi-centennial climate variability during the past two millennia, the Common Era (CE), despite the apparently small changes in external forcings. Proxy records suggest that the Northern hemisphere (NH) was about 0.8 °C cooler during the Little Ice Age (LIA, 1450-1850 CE) relative to the Medieval Climate Anomaly (MCA 950-1250 CE) and the last century. The majority of these anomaly reconstructions are from terrestrial records in the NH while information from the Indo-Pacific Warm pool (IPWP) are limited. As the latter exert strong influence on atmospheric convection and thus global climate and rainfall studying the climate of IPWP during the CE can help discern natural variability as well as anthropogenically forced alterations.

Here I use planktonic foraminifera in rapidly accumulating sediments to reconstruct sea surface temperature (SST) and salinity in the Indonesian Seas to investigate changes in tropical temperature anomalies and monsoon strength throughout the CE. I have studied two sediment cores, one in the northern Makassar Strait, and the other in the Java Sea. The reconstruction of climate parameters is obtained by measuring magnesium/calcium ratios (Mg/Ca) and the oxygen isotopic ($\delta^{18}O$) composition in the tests of a surface dwelling foraminifer, *Globigerinoides ruber (sensu stricto)*. The combined multi and gravity cores exhibit a significant trend in SST from northern to southern Makassar strait, suggesting significant local variability superimposed on the regional and global signals. A compilation of my Makassar Strait records with previously published records shows a 0.60 ± 0.25 °C cooling in the LIA and temperatures about as warm as the reference period (1860-1890 CE) during the MCA which is highly correlated with the NH temperature reconstruction. Model output showing the SST variability with forcing parameters held constant in the same region show ± 0.25 °C unforced variability leaving evidence that the SST variability in the proxy compilation could be externally forced.

Paired measurements of Mg/Ca-SST and $\delta^{18}O_{calicte}$ data are used to derive the $\delta^{18}O_{sw}$, a proxy for salinity which shows more depleted values in sites south of the equator during the LIA, interpreted as fresher conditions. This apparent freshening of the surface water suggests enhanced precipitation associated with the Indonesian boreal winter monsoon.

Acknowledgements

I would first like to thank my advisor, Yair Rosenthal, for taking a risk to hire me and then encouraging me to pursue graduate studies. I appreciate all the geochemical tools, and proper laboratory technique that I have learned from him.

I'd also like to thank my committee members Anthony Broccoli and Braddock Linsley for their support and ideas to progress the science in this thesis.

Although not officially part of my committee, Delia Oppo has so generously given her time and scientific input at various stages of my research. From her suggestions I have learned a lot.

Jim Wright and Rick Mortlock provided stable isotope measurements at Rutgers and well as scientific and career advice. Braddock Linsley performed some isotope measurements as well. Thank you all for your help and quality data.

I would like to thank Robert Sherrell for the amazing opportunity to go on the Antarctic expedition and learn trace metal clean water sampling and processing techniques. This was a once in a lifetime experience and I cannot thank you enough for allowing me to go with you!

Also on the Antarctic expedition was Silke Severmann. I am so grateful for having you as a teacher, for our intellectual discussions whether scientific or otherwise, your creativity (even though sometimes a few harmless delectable gummy treats may be injured in the process), your sassy attitude, and course giving me and Callie (woof, woof) a home my last few months!

Liz Sikes, I would like to thank you for being a great role model of women in science with a family and of course for some fabulous geochem grrrrrlls dinners!

Robert Chant, I am not sure whether to thank you or curse you for introducing me to Hungarian hot dogs! Thank you for having me over for several good meals and great conversations over beer or coffee, two vices we both enjoy!

Babila, Babs, TALLEY, you are obvi a totes rad dudette! Selfishly I was thankful that when I had a really stressful semester you always did too which meant I had a buddy to commiserate with and eat dinner with in the office suite! Your friendship and moral support has meant more to me than I could ever express! I couldn't have made it without you!

Julie, you are truly the sweetest person I have ever met. Thank you for always being a good listener, a great cheerleader, and an incredibly helpful labmate! Thanks also for those amazing NYC evenings!

Anna Hermes, somehow you made going into work on the weekends "fun" as long as we did it together! Your drive and motivation inspired me to be better. Your advice and friendship has kept me going for the past three years. How could we have done graduate school with those *essential* Target and DD runs! And honestly, who else can take an ordinary baseball helmet and make it into a bob sled and astronaut costume! ☺

A special thanks, to Audrey Morley for her intellectual insight, advisement and encouragement throughout my second year. Your help has been invaluable!

I would like to thank Julie Criscione for being a wonderful undergraduate to work with and very helpful in the lab. Also, Micheal Erb for his help extracting the model data.

To my family, I would like to thank you all for your emotional support. In particular, my broseph, his encouragement throughout the years has not been overlooked; I could not have done this advanced degree without his example!

I would also like to thank Adam for his patience, support and encouragment throughout AGU and the writing process. I know his idea of quality time does not include having dinner in room 203 but I appreciated every minute we spent together!

For friendship, dog sitting, emotional support and office giggles I thank the following people; Jeana Drake, Mikaela Provost, Maria Lagerström and Stella Woodward.

Finally this work would not have been possible without funding from the National Science Foundation Grants. The Indonesian Agency for Assessment and Application of Technology (BPPT), the Center of Research and Development for Oceanography (LIPI) of Indonesia and the Captain as well as crew of the 2003 RV Baruna Jaya VIII cruise for providing support to get the samples used in this project. Also I would like to thank the Institute of Marine and Coastal sciences for funding my studies, giving some additional support for conference costs, and exposure to some diverse and exciting research!

Table of Contents

List of Tables

List of Figures

1. Introduction

In order to understand recent warming in context of natural variability past reconstructions of temperature have been complied from the Common Era (CE). Several temperature proxy compilations spanning the CE are available for the northern hemisphere (NH) during the Medieval Climate Anomaly (MCA, 900-1250 CE) suggesting that temperatures were about the same as, and during the Little Ice Age (LIA, 1450-1850 CE) temperatures were about 0.6 -0.8 °C cooler than the reference period (1961-1990 CE) [*Mann et al.*, 2009; *Moberg et al.*, 2005]. Comparisons with the southern hemisphere (SH) and tropics are limited due to the sparse proxy records in the years preceding 1700 CE of decadal or greater resolution [*Neukom and Gergis*, 2011]. For this reason the uncertainty about the global response to these centennial climate anomalies is still relatively large [*Mann et al.*, 2009]. It is important to have more decadally-resolved records with large geographical coverage to compare with the trends seen in the NH.

Of special interest is, the Indo-Pacific warm pool (IPWP) which is characterized by the warmest mean annual sea surface temperatures (SST) <28°C about 2-5 °C higher than any other equatorial region [*Yan et al.*, 1992]. Changes in the IPWP surface temperature appear to closely follow those of global averages [*Oppo et al.*, 2009] and therefore play an important role in modulating the global climate [*Meyers et al.*, 1986]. In particular, variations in SST of the IPWP affect the strength and location of Hadley circulation and thus tropical hydrology [*Neale and Slingo*, 2003] although this can also be influenced by alterations in high latitude temperatures [*Broccoli et al.*, 2006].

To date only one compilation based on limited number of marine records is available for the IPWP [*Oppo et al.*, 2009] and none for the Eastern Equatorial Pacific. The strength in these reconstructions is that they span the entire CE and are of multi-decadal to centennial resolution, however, all 3 records come from a very small region and therefore could reflect local conditions from the central Makassar Strait. To broaden the scope of this reconstruction and discern local from larger scale variability I add two new records, one in the northern Makassar Strait and the other in the Java Sea to decipher the complexity of SST variability in this region. In particular, I look at the influence of monsoons and thus surface currents at each individual site through the CE to determine if some locations are more representative of the IPWP or local monsoon variability. After discerning the local variability, I compile the five SST records of multi-decadal resolution to compare with the NH reconstructions with greater confidence. I also present a comparison of this new compilation with a model study where the external forcing parameters are held constant revealing the expected SST variability with no climate forcings. The records and compilations that are produced in this study will aid in understanding the SST and salinity variations through the CE in the IPWP.

2. Oceanographic Setting

On the western side of the equatorial Pacific Ocean, the Indonesian Seas are a conduit between the Pacific and Indian oceans and play an important role in transporting heat between the two oceans. The major current known as the Indonesia Through Flow (ITF) exports 13 Sv of water or 10^6 m^3/s from the Pacific ocean and 2 Sv from the Indonesian Seas into the Indian Ocean on average per year [*Gordon et al.*, 2010]. The Lombok Strait, Ombai Strait and the Timor Passage are the major outflows of the ITF depicted in Figure 1 with red solid arrows [*Gordon et al.*, 2010]. Initial research suggests that a combination of local wind patterns and the pressure gradient due to the difference in sea level pressure from the Philippines to the Australia are the driving forces of the ITF [*Wyrtki*, 1961; 1987]. Although the pressure gradient between the two oceans is persistent through most of the year, it is not a significant influence on the total ITF transport [*Burnett et al.*, 2000]. Rather the ITF is an extension of the large-scale flow of the Pacific and Indian oceans [*Mayer et al.*, 2010]. During boreal winter the Mindanao Current, the western edge of the North Equatorial Current (NEC), interacts with the Philippine Islands creating an eddy that rotates clockwise which will propagate westward through the ITF [*Mayer et al.*, 2010]. In boreal summer when the New Guinea Current, part of the South Equatorial Current (SEC), reaches the Halamahera Sea a counter clockwise eddy is produced and since in the SH that will propagate westward as well [*Mayer et al.*, 2010]. In essence the pressure gradient between to the two oceans can influence transport but the reason for the existence of the ITF is due to the interactions of the Pacific current system with the islands in this region [*Mayer et al.*, 2010].

Temperature and salinity patterns of the Indonesian Seas vary seasonally due to the strong influence of the monsoons in this region. In boreal summer (July to September) the Southeast Asian Monsoon drives water from the Banda and Flores Seas into the South China Sea through the Karimata Strait [*Qu et al.*, 2005]. This will be referred to as the Indonesian boreal summer monsoon (IBSM). The outflow of water from these seas induces upwelling of cold water which is evident by cooler SST of sites in the southern Makassar and Java Sea by ~1.5°C (Fig. 2) [*Qu et al.*, 2005; *Wyrtki*, 1961]. Due to the strong subsurface flow through the Makassar Strait the cool surface flow from the Java Sea into the Makassar Strait is hindered allowing SST at sites in the northern Makassar to remain warm ~29°C [*Gordon et al.*, 2003]. While the SST at the different sites from north and south of the Makassar vary during the IBSM monsoon the salinities remain similar [*Newton et al.*, 2011] (Fig. 2). With the onset of the Northwest Asian Monsoon in boreal winter (January to March) the winds drive cool fresh water from the South China Sea through the Karimata Strait and into the Java Sea, this will be referred to as the Indonesian boreal winter monsoon (IBWM) [*Gordon et al.*, 2003; *Wyrtki*, 1961]. This input of less saline water creates a salinity gradient between the north and south Makassar strait inhibiting the surface flow of water from the Pacific Ocean through the Makassar Strait [*Gordon et al.*, 2003; *Newton et al.*, 2006] (Fig. 2, Fig. 3). The SST between all the core sites during the IBWM monsoon is more similar (28.5 – 29.5°C) than during the IBSM monsoon. In summary the southern cores experience significant seasonal variability and the northern cores do not.

3. Materials and Methods

3.1 Cores Location

I generated records on two primary sites; one located in the Bali Basin near Lombok Strait and the other near the delta of the Mahakam River on the Eastern side of the northern Makassar Strait (Table 1; Fig. 1). At each site I sampled a multi-core which recovered the most recent period overlapping the instrumental record and a gravity core allowing us to extend the record for the whole CE. The cores located in the Bali Basin are named BJ8-03 7GGC and 6MC and are referred to here as BJ-7 for the whole record or BJ-6 for just the top 45 cm. The cores in the northern Makassar are named BJ8-03 85 GGC and 84MC and are referred to as BJ-85 for the whole record or BJ-84 for just the top 45 cm from now on. Mean annual SST from 1998-2008 near BJ-7 is ~28.7°C whereas near BJ-85 SST averaged values are ~29.3°C [*Smith et al.*, 2008]. As mentioned above, the IBSM creates upwelling in the Java and Flores Sea that lowers SSTs, which predominantly affects BJ-7 over BJ-85 (Fig 2). During the IBWM, surface waters are freshest in both locations from the entrainment of South China Sea water and also rain associated with the southward migration the Intertropical Convergence Zone (ITCZ) [*Aldrian and Dwi Susanto*, 2003; *Xie and Arkin*, 1996].

In addition we took a third multi-core in the semi-closed basin of the Teluk Saleh. This basin has a sill depth of ~100m which allows exchange with the surroundings seas through the thermocline. Sumbawa Island, home of Mt Tambora, is the landmass enclosing this body of water. Mt Tambora had an incredibly explosive eruption in 1815 consequently known as the year without a summer

[*Stothers*, 1984]. As a result of the large amounts of tephra emitted into the atmosphere, which then were deposited on the ocean floor, an impenetrable ash layer was reached at the bottom of the multi-core when attempting to core this location. For this reason no gravity core was collected at this location.

As part of the compilation, already published records from the northern and Mid-Makassar are used [*Newton et al.*, 2006; *Newton et al.*, 2011; *Oppo et al.*, 2009]. The core the farthest north is MD98-2177 (1˚ 24'N, 119˚ 05'E, 968m; referred to as MD-77), followed by BJ8-03 34GGC, 32GGC & 31MC a little south of that (3˚ 53'S, 119˚ 26'E, 503m; referred to as BJ-34 for the whole record or BJ-31 for just the top 50 cm) and finally MD98-2160 located in the southern Makassar (5˚ 12'S, 117˚ 29'E, 1185m; referred to as MD-60) (Fig. 1).

3.2 Analytical Methods

After recovery, the multi-cores are sampled in quarter round sections at intervals of every centimeter. BJ-7 is sampled every centimeter from 0-100cm and then every 4 cm from 100-200cm where BJ-85 is sampled every 2 cm from 0-100 cm followed by every 4 cm for the next 100 cm. Once the mud samples are washed through a 63 μm sieve to remove the fine sediment fraction, the surface dwelling planktonic foraminifera *Globigerinoides ruber* sensu stricto morphotype (*G. ruber s.s.*) are picked from both the 212-250 μm and 250-300 μm size fractions for isotopic and trace element analyses, respectively. Sediment trap series in the IPWP suggest *G. ruber* s.s. lives throughout the year in constant abundance making it an ideal species to reconstruct mean annual SST [*Mohtadi et al.*, 2009].

3.2.1 Trace Element Analysis

Thirty to forty *G. ruber* tests from the 250-300 μm size fraction are crushed and then cleaned using a modified protocol (*Rosenthal et al.* [1997]) to remove clays, organic matter and metal oxides *Boyle and Keigwin* [1987]. The cleaned tests are dissolved in trace metal grade 0.065 N HNO_3 (Optima) and 100 μL of dissolved sample is diluted with 300 μL trace metal clean 0.5N HNO_3 to obtain a Ca concentration of 4 ± 1mmol/L. Samples are analyzed by Thermo Element XR Sector Field Inductively Coupled Plasma Mass Spectrometer (SF-ICP-MS) operated in low resolution ($m/\Delta m = 300$) following the method outlined in *Rosenthal et al.* [1999]. Direct determination of elemental ratios from intensity ratios is significantly affected by the sample Ca concentration of the solute. In order to correct for this matrix effect, six standard solutions with identical elemental ratios but variable Ca concentrations are included in each run where the range in Ca concentrations is 1.5-8 mM. These solutions allow us to quantify and correct for the effects of variable Ca concentrations in sample solutions on the accuracy of Mg/Ca measurements or matrix corrections as outlined in *Rosenthal et al.* [1999] and *Andreasen et al.* [2006]. These corrections are typically small, <0.1 mmol/mol Mg/Ca.

Instrument precision is determined by repeat analysis of three consistency standards over the course of this study. Long term analytical precision of the consistency standards with Mg/Ca of 1.24 mmol/mol, 3.32 mmol/mol and 7.5 mmol/mol are ±0.62%, ±0.50% and ±0.70 % respectively (Appendix Fig. 2).

Contamination is monitored by measuring Mn/Ca, Fe/Ca, and Al/Ca. Incomplete removal of sediments containing metal oxides inside the test chambers is apparent when the Fe/Ca and Al/Ca values are anomalously large. High Mn/Ca values are an indicator of Mn-carbonate overgrowths. Threshold values for these elements in the Indonesia region are the following; Mn/Ca 250 μmol/mol, Fe/Ca 2000 μmol/mol and Al/Ca 2000 μmol/mol (See Appendix). In addition to contamination limits, a sample is also discarded if the calcium value is below 0.6 mmol/L due to detection limits on other trace elements when the calcium is low.

3.2.2 Isotope Ratio Analysis

Carbon and oxygen isotopic analysis is performed on 12-15 individuals from the 212-250 μm size fraction by reacting with 100% H_3PO_4 at 90°C in a multiprep carbonate preparation device. The resulting CO_2 is analyzed with Micromass Optima Dual-Inlet mass spectrometer. BJ-7 and BJ-142 are measured at the University of Albany State University of New York and Lamont-Doherty Earth Observatory with Dr. Braddock Linsley. Over the last several years the standard deviation of the National Institute of Science and Technology international reference standard (NBS19) is 0.04‰ for $\delta^{18}O$. BJ-85 is measured with Dr. Jim Wright at Rutgers University Department of Earth and Planetary sciences with the same setup. Long term precision at Rutgers for $\delta^{18}O$ and $\delta^{13}C$ is 0.08‰ and 0.05‰ respectively. An internal standard that is calibrated against NBS19 is used where the offset between the two is 0.04‰ and 0.01‰ for $\delta^{18}O$ and $\delta^{13}C$. See appendix for a table of this data or Figure 4 for the plots of the raw data.

Mg/Ca-based temperature estimates and $\delta^{18}O_{calcite}$ data from the same depths are used to calculate $\delta^{18}O_{sw}$. The *Bemis and Spero* [1998] calibration is used where T(°C) = 16.5 – 4.80($\delta^{18}O_{calcite}$ - $\delta^{18}O_{sw}$) - 0.27‰. Since the ice volume change during the Common Era is minimal and would not alter tropical $\delta^{18}O_{sw}$ this correction is not applied.

3.3 Chronology

Multi-cores allow retrieval of the top ~50 cm of sediment with minimal compaction and almost no disruption in the stratigraphy. In my sites, this allows for correlation with the instrumental record and also the use of dating techniques limited to the past 100 years such as lead isotopes (^{210}Pb) and correlation to the Suess Effect [*Keeling et al.*, 2008; *Swart et al.*, 2010]. All ^{14}C dates are calibrated to calendar years using the 'Fairbanks0107' calibration curve [*Fairbanks et al.*, 2005].

The decrease in $\delta^{13}C$ at the top of BJ-84 is consistent with the recent atmospheric drop due to the dilution of isotopically enriched carbon from the burning of fossil fuels [*Swart et al.*, 2010]. This trend is also seen in BJ-31 which has a well defined age model therefore the top of BJ-84 was correlated to BJ-31 [*Oppo et al.*, 2009](Fig. 4). Using the tie points from BJ-31 in the first 7 cm of the record and the ^{14}C date near the bottom of the core an age model is constructed that has an error of ±60 years due to the errors in the ^{14}C date.

The top of BJ-6 is correlated with BJ-31 using the $\delta^{13}C$ values in a similar manner as BJ-84. Another tie point at 25.5 cm is the ash layer attributed to Mt Tambora's eruption in 1815 (Table 4). This ash layer is detected by measuring the percent coarse fraction relative to the total sediment fraction where a value greater then 15% was indicative of ash. Using these two points a sedimentation rate of 134 cm/kyr is determined. Assuming a linear sedimentation rate the age at a depth of 43.5 cm is determined to be 1680 CE or 270 BP. The ^{14}C age at this depth is 745 ^{14}C years with an error of ±30 yr. By using a range of reservoir age corrections from 450 to 530 years the closest to an age of 1680 CE after conversion to calendar age is achieved when using a reservoir age correction of 510. For this region, reservoir age corrections of 400-475 years are used, [*Linsley et al.*, 2010; *Newton et al.*, 2011; *Oppo et al.*, 2009] yet I found a reservoir correction of 510 to be most accurate therefore given age uncertainties I rounded this correction to 500 years. The error from this age model is the error in the ^{14}C dates, which is ±50 yr.

For the remaining multi-core, BJ-142, ^{210}Pb isotopes are measured on this core and a near by multi-core (BJ8-03 146 MC) where the data is shown in Table 3. These ^{210}Pb dates allow for accurate sedimentation rates and ages to be determined in the top 10 cm. In addition, this core is near the site of Mt. Tambora where the bottom of the core reached the impermeable ash layer form the 1815 eruption. Combining these dates enables an age model with an error of ±15 years.

The age models for the gravity cores BJ-7 and BJ-85 are constructed using ^{14}C dates with the newly determined reservoir correction of 500 years (Table 2). In addition to radiometric dating BJ-7 also contained ash from the Mt. Tambora eruption giving a tie point for the top of the core and also good overlap with its companion multi-core. The error in the age model for BJ-7 is on the order of ±40 yr due to average error in the five ^{14}C dates. Five radiocarbon dates are used to construct the age model for BJ-85, one of which simply reveals that the top is modern. The top of the core is correlated with BJ-84 using $\delta^{13}C$ values where the

0.3‰ drop reflects the Suess Effect. The remaining four dates when converted to calendar age are used to construct the age model for the rest of the core leaving an age error of ± 60 years. The average sedimentation rate for BJ-7 and BJ-85 throughout the core is ~70cm/kyr which made it capable to look at decadal to multi-decadal trends throughout the CE.

3.4 Instrumental SST

In this study I use National Oceanic and Atmospheric Administration extended reconstructed SST (ERSSTv3) to compare with the proxy data [*Smith et al.*, 2008]. ERSSTv3 data is monthly averaged SST on a 2° degree grid taken from the Comprehensive Ocean-Atmosphere Data Set (CODAS) composed of ship and buoy SST observations. Since there are limited observations from 1856-1900 in the IPWP, the ERSSTv3 values from 1900-2000 CE are used.

In order to compare these observations with the proxy records a 4x4 degree grid box centered at each core site was extracted. From one 4x4 grid box or the nine data observation sites, the monthly values are averaged to yield one SST measurement per year.

3.5 Temperature Anomaly Compilation

I also complied previously published Mg/Ca data from planktonic foraminifera from cores located in the Makassar Strait (Fig. 1). All records are based on data from *G. ruber* and converted to temperature using the *Anand et al.* [2003] multi-species calibration.

Temperature anomalies for the combined multi and gravity cores at site BJ-7 are calculated by averaging the SSTs from 1860-1890 CE and subtracting that value from each SST in the record. This is performed on all the records used in the compilation; BJ-85 (this study), BJ-34 [*Oppo et al.*, 2009], MD-60 and MD-77 [*Newton et al.*, 2011] (Fig. 8). The reference period of 1860-1890 CE is chosen because all of the five proxy records in the compilation had data during this interval.

To make the compilation all records from 860-1920 CE are interpolated to 20 year intervals and the five records averaged every 20 year time step and then smoothed to 80 years (Fig. 12). From 40-840 CE the records are interpolated to 40 years then the four records averaged (excluding BJ-85) and smoothed to every 160 years. Due to the low sample resolution of BJ-85 after 800 CE it is not included in the second half of the compilation. To test that the compilation is robust and not influenced by one location more than another the "Jack-knife" approach is performed [*Efron*, 1982]. The procedure for this is to make the compilation omitting one record each time to see the difference between this compilation and the whole composite (See appendix Fig. 1).

3.6 Climate Model series 2.1 Compilation

Model results from the Geophysical Fluid Dynamics Laboratory (GFDL) Climate Model 2.1 series (CM2.1) are used to look at unforced SST variability at the core sites compiled in this study [*Delworth et al.*, 2006]. The CM2.1 experiment is a global coupled ocean-atmosphere model with forcing agents consistent with year 1860 CE. The forcings are held constant through the run in order to assess SST variability due to internal mechanisms without external perturbations to the climate system. The forcings included in this model are the following; the well-mixed greenhouse gases (CO_2, CH_4, N_2O), tropospheric and stratospheric O_3, tropospheric sulfates, black and organic carbon, dust, sea salt, solar irradiance and the distribution of land cover types. In essence the CM2.1 experiment is a control run set with preindustrial (1860) climate forcing parameters.

SST data is extracted from a location near each core site at 3 depth levels of 5m, 15m and 25m (Table 5). Temperature anomalies are computed by averaging the last 30 years of the model data and then this value is then subtracted from each point in the entire run. This is performed for each core site and each depth individually (Fig. 10). The anomalies at each core site from the three depths are then averaged into one anomaly for that location representing the upper mixed layer 5-25m (Fig. 11). Finally the depth averaged anomalies at each core location are averaged together to make a composite similar to the proxy data compilation (Fig.12).

3.7 Calculating error on SST reconstructions

Mg/Ca values are converted to temperature using the Anand multi-species equation: Mg/Ca = b $\exp^{(aSST)}$ where a =0.09 and b= 0.38 [*Anand et al.*, 2003]. In this calibration, the pre-exponential and exponential constants have standard errors of b = ±0.02 and a = ±0.003, respectively . As a result, the reported standard error in Mg/Ca temperature estimate is 1.2 °C [*Anand et al.*, 2003]. The standard error on replicate analysis is ±0.5 °C which includes the error associated with cleaning protocols and the small analytical precision error of ±0.1 °C (see section 3.2.1). Combined the standard error for an individual SST estimate is ± 1.3 °C. The error in the 3 point smoothed absolute temperature reconstruction is determined by taking the above error divided by the square root of n-1 where n is the number of points that are smoothed.

Absolute Temp Error: $[(1.2)^2 + (0.5)^2]^{1/2} = \pm 1.3$ °C

Smoothed Absolute Temp Error: 1.3 °C $/(3-1)^{1/2} = \pm 0.9$ °C

The error in the anomaly calculations is smaller since in that case only the relative temperature change, not the absolute temperature, is calculated. Essentially from the calibration only the standard error of the exponential constant (a) is needed where an error of ±0.003 relates to a ±0.9 °C. The other errors are the same from above, but the temperature anomalies were smoothed by 4 points leading to the equations and errors below.

Temp. Anomaly Error: $[(0.9)^2 + (0.5)^2]^{1/2} = \pm 1.0$ °C

Smoothed Anomaly Temp Error: 1.0 °C $/(4-1)^{1/2} = \pm 0.6$ °C

Finally for the compilation (Fig. 12) the temperature anomaly error is still ±1.0 °C but since five records were compiled with 4 points smoothing from 1920-880 CE the error reduces to ± 0.23 °C one standard error. From 840 – 40CE since only four records were complied the standard error is ± 0.26 °C shown below.

Sm. Anom. Temp. Error (1980-880 CE): 1.0 °C $/((4*5)-1)^{1/2} = \pm 0.23$ °C

Sm. Anom. Temp. Error (840- 40 CE): 1.0 °C $/((4*4)-1)^{1/2} = \pm 0.26$ °C

To validate the selection of calibration I compare smoothed Mg/Ca-derived SST with smoothed ERSSTv3 (Fig. 5). Here I show that the instrumental SSTs are well within the one sigma standard error, (± 0.9 °C), of the proxy reconstructed SSTs.

4. Results and Discussion

4.1 Trends in Mg/Ca-SST and $\delta^{18}O_{calcite}$

Site BJ-6 has a ~2°C warming trend, equivalent to an increase of 1 mmol/mol Mg/Ca, where ~1°C occurs from 1700-1880 CE with the rest of the warming from 1880-2000 CE (Fig. 6A). BJ-142, consistent with BJ-6, shows a ~1°C warming from 1900-2000 CE (Fig. 6A). Warming of ~1°C also occurs in the published multi-core *Oppo et al.* [2009] at site BJ-31, yet BJ-85 has no evident warming or cooling in the past 3 centuries. Coral proxy records from the IPWP show similar warming trends of 0.5- 1.0°C from 1880- 2000 CE [*Cobb et al.*, 2003; *Guilderson and Schrag*, 1999; *Hendy et al.*, 2002; *Nurhati et al.*, 2011; *Wilson et al.*, 2006]. However, tropical Pacific temperatures are influenced by natural phenomena like the El Niño Southern Oscillation (ENSO) and the Pacific Decadal Oscillation (PDO) making interpretations of temperature alterations complicated [*Cobb et al.*, 2003; *Y Zhang et al.*, 1997]. Yet the overall warming trends seen in 12 locations across the tropical Pacific into the twentieth century suggest a response that may be caused by anthropogenic greenhouse forcings [*Nurhati et al.*, 2011]. The warming seen in the coral records is consistent with trends seen in the multi-cores from this study, adding more evidence to an anthropogenically forced warming in the tropics (Fig. 5).

In all multicores the $\delta^{18}O_{calcite}$ values are varying by ±0.4 ‰ with no long term trend (Fig. 6A). Given that oxygen isotopes are influenced by temperature as well as evaporation and precipitation, the lack of a trend similar to the Mg/Ca derived SST in the $\delta^{18}O_{calcite}$ may suggest a change in salinity. The $\delta^{18}O_{sw}$ values for BJ-31 and BJ-6 show more saline conditions in the twentieth century than preceding ones as the values increase by 0.4 ‰ (Fig. 6B). BJ-142 also shows a trend toward saltier conditions while BJ-84 has no long term trend (Fig. 6B). *Tierney et al.* [2010] also show drier conditions in last 30 years from their δD leaf wax record at site BJ-31 and from the Indonesian instrumental isotopic rainfall data from Global Network of Isotopes in Precipitation (GNIP) although the magnitude is different; the instrumental record shows an enrichment of ~20‰ compared to their record of ~6‰. While interpreting the $\delta^{18}O_{sw}$ records as alterations in salinity induced by rainfall appears to be consistent with previous records for the region this proxy might be affected by advection and not solely an indicator of rainfall. For this reason other proxies like δD may be more reliable for precipitation changes.

The spliced multi-gravity core records at site BJ-7 demonstrate a ~2.5°C long term cooling trend from 500 CE to 1700 CE with a plateau from 900-1100 CE, which is then followed by an accelerated warming of ~2°C from the end of the LIA into the twentieth century (Fig. 7). The cooling trend into the LIA seen in BJ-7 is similar to previously published records MD-60 and BJ-34 but the onset of the cooling starts about 1000 CE whereas in the other records it begins around 1200 CE (Fig. 8). The site located in the northern Makassar Strait, BJ-85, shows a cooling trend of ~1°C starting around 900 CE into the LIA but does not have persistently colder temperatures than the reference period (1860-1890 CE) throughout the LIA unlike the sites located in the southern Makassar Strait and the Java Sea (Fig. 8). In all the records the MWP is not as prominent as the LIA, where on average the temperatures are about as warm as the reference period (1860-1890) to 0.5 °C warmer.

In general over the Common Era the three published records and two from this study demonstrate larger SST variability at sites in the Southern Makassar (MD-60, BJ-34, BJ-7) than in the Northern Makassar (MD-77, BJ-85) (Fig. 1; Fig 8). On a seasonal basis the instrumental SST records show that the southern sites have a ~2°C degree temperature range whereas the northern sites have less than 1°C change suggesting that the southern sites are more sensitive to local current systems than the northern sites (Fig. 2). Yet the reconstructed SST are representing a mean annual SST not a seasonal cycle [*Mohtadi et al.*, 2009]. The larger SST variability through the Common Era in the southern sites might reflect modification in the strength of the monsoons. The boreal summer monsoon in the NH is called the East Asian summer monsoon (EASM) whereas the boreal winter monsoon in the NH is called the East Asian winter monsoon (EAWM). The boreal summer monsoon in the SH will be referred to as the Indonesian boreal summer monsoon (IBSM) and the boreal winter monsoon in the SH referred to as Indonesian boreal winter monsoon (IBWM).

Another possibility could be that during the LIA the IBSM is strengthened causing more intense upwelling in the Java Sea consequently cooling the southern sites while the northern sites remain unaffected. Yet another scenario is that during periods of NH cooling like the LIA the IBWM is strengthened causing enhanced flow of cool water from the South China Sea into the southern Makassar Strait which would also just cool the southern sites.

Subtropical (Waxaing Cave) and coastal southeast China (Lake Huguang Maar) proxy data have shown during periods of NH warmth MCA, Roman Warm

Period (RWP) the EASM is stronger and the EAWM weaker [*Yancheva et al.*, 2007; *P Zhang et al.*, 2008] (Fig. 9). The anti-correlation between these two NH monsoons is due to the migration of the ITCZ which follows NH temperatures such that when the NH is warm (cold) the ITCZ is in a northerly (southerly) position [*Broccoli et al.*, 2006; *Haug et al.*, 2001; *Sachs et al.*, 2009; *Tierney et al.*, 2010]. On centennial timescales northerly shifts of the tropical rain belt toward China on a mean annual basis would weaken the EAWM [*Yancheva et al.*, 2007]. Conversely, during episodes of NH cooling, when the ITCZ is in its southerly position residing over Indonesia the IBWM is strengthened, [*Oppo et al.*, 2009; *Tierney et al.*, 2010]. In essence centennial migrations of the ITCZ are modulated by heat disparity between the two hemispheres where northerly shifts strengthen the EASM while weakening the IBWM [*Tierney et al.*, 2010].

During the LIA the IBSM would be weakened therefore enhanced upwelling is most likely not the cause of the LIA cooling seen at the sites in the southern Makassar[*Oppo et al.*, 2009; *Tierney et al.*, 2010]. More coherent is the suggestion that during episodes of NH cooling the IBWM is strengthened which would augment the flow of cool water from SCS to the Java Sea lowering the SST at southern sites but not the northern ones [*Oppo et al.*, 2009] (Fig. 8). The significant cooling of ~1.5 °C during the LIA at these sites might be due to the cooling of North Pacific water which enters the South China Sea and then these sites through the Karimata Strait [*Oppo et al.*, 2009]. The sites in the northern Makassar Strait receive water primarily from the WPWP through the NEC (boreal summer) and SEC (boreal winter) and are not as influenced by monsoonal driven currents [*Mayer et al.*, 2010].

4.2 CM2.1 SST and Proxy SST Compilation

The CM2.1 control experiment shows unforced temperature variability at all the core sites for the 500 years of the model run (Fig. 10). For all sites there is greater amplitude in variability at the depth of 25 m which is most likely due to upwelling and alterations in the thermocline depth (Fig. 10). The depth averaged (5-25m) temperature anomalies at each core site show minimal variation once smoothed (Fig. 11). These results suggest that the unforced variability at these sites is minimal (±0.25 °C) with no long term trend (Fig. 11). Since the temperature ranges seen in the IPWP compilation from this study are larger than those from the CM2.1 model compilation this would imply these temperatures are externally forced, assuming that the model is realistic (Fig. 12). The IPWP proxy compilation mimics the Mann et al., (2009) NH temperature reconstruction quiet well suggesting that the temperature trends were not limited to the NH (Fig. 12).

In the late Holocene the boundary conditions of the climate system did not change as dramatically as they had from glacial to interglacial times [*Wanner et al.*, 2008]. This in part is due to the short timescale of this period compared to the long cyclicity of some external forcings like orbital variability. The major forcings for the Common Era, the past 2,000 years, that could affect millennial or multi-centennial timescales are volcanic eruptions, solar variability and the anthropogenic rise of carbon dioxide (CO_2) [*Wanner et al.*, 2008].

The LIA coincides with the Maunder Minimum, a period from 1645-1715 that appeared to interrupt the normal course of the solar cycle with minimal sunspots and therefore decreased solar activity, as can be seen in Figure 13 [*Bard et al.*, 2000;

Eddy, 1976; *Lean et al.*, 1995; *Steinhilber et al.*, 2009]. Previous work has shown that correlations of NH temperature anomalies complied from Bradley and Jones (1993) with solar activity from the period 1610-1800 are 0.86 (r^2) suggesting that the dominant control on climate during this period was probably solar [*Lean et al.*, 1995]. However, the mechanisms involved in solar-climate relationships are still not well understood [*Beer et al.*, 2006] and in particular how an alteration of a 0.2 W/m^2 or 0.1% in solar irradiance (ΔTSI) would alter global temperatures [*Lean et al.*, 1995]. With that caveat in mind, the compilation from this study is suggesting a similar timing and amplitude of cooling as the NH during the LIA, a period when the only climate forcing that changed for persistent periods was solar (Fig 12) [*Bard et al.*, 2000; *Eddy*, 1976; *Lean et al.*, 1995; *Steinhilber et al.*, 2009].

The other potential climate forcing is from explosive volcanic eruptions which release large volumes of aersols like SO_2 and H_2S into the atmosphere that have the capability of cooling the earth's surface by 0.1-0.3 °C [*Zielinski*, 2000]. The climate feedbacks from volcanic events depending on the size of the eruption can range from affecting a small region to the entire globe. From volcanic aerosol reconstructions it appears that there were a few events throughout the LIA which may have aided in the cooling of the tropics [*Crowley*, 2000] (Fig. 13). Volcanic events are, however, short lived and therefore their impact on SST may not be resolved in this study. Yet the combined effect of diminished solar activity and increased tropical eruptions during the LIA may have caused the 0.5 -0.7 °C cooling seen in this compilation (Fig. 13).

In addition to understanding the mechanisms of cooling in the Indonesian seas it is crucial to ascertain what the SSTs in this region are representing. For example, whether the reconstructed SSTs for this region reflect local temperature variability at each site or show temperature alterations indicative of the tropical Pacific. If the southern sites (BJ-7, MD-60 & BJ-34) are indeed influenced by North Pacific water during the IBWM and South Pacific water during IBSM these sites may not truly representat the WPWP hydrography. On the other hand, it is possible that an enhanced "freshwater plug" [*Gordon et al.*, 2003] inhibited the southward surface ITF flow thereby leading to local warming at the Northern sites (BJ-85 & MD-77). For this reason it is important to look at the compilation in a few ways with all the sites, with just the northern sites and then with just the southern sites shown in Figure 14.

The northern compilation shows multi-decadal variabilty ± 0.5 °C SST variability with no persistent trend towards warmer or cooler temperatures for a time interval longer than a century (Fig. 14). Conversely, the southern sites show a distinct cooling trend during the LIA of 0.5-0.8 °C (Fig. 14). This disparity may arise due to the locations of each site. From the monsoonal driven surface currents there is minimal flow of water from the south Makassar to the north Makassar which separates what water masses the northern and southern sites are representing. In addition, the Makassar Strait is constrained by a shallow sill, about 400 m, with a narrow channel that transports water from the north to the south which inhibits the flow of water in the south to north direction of the strait [*Gordon et al.*, 2010]. Therefore the SST of the southern sites may not be representative of the WPWP where the northern sites are, given that their source water is directly from the WPWP [*Mayer et al.*, 2010]. If this is true than the northern SST compilation which may be representative of the WPWP shows minimal temperature variation throughout the LIA and MWP. This could suggest that the Pacific tropical region is not as sensitive to small variations in solar activity or volcanic eruptions as the northern hemisphere.

5. Conclusions

The Northern Makassar Strait sites experience little SST variability throughout the Common Era and might be more representative of the WPWP than the southern sites which are influenced by monsoonal activity. When all compiled, however, there is great coherence with the NH temperature reconstructions suggesting these SST changes may be externally forced and not limited to high latitudes. The CM2.1 model study, assuming that it is representative, supports that idea the SST variability from the reconstructed data is greater than unforced variability.

The "salinity" reconstruction at BJ-7 suggests a strengthening of the IBWM due to the southern migration of the ITCZ during periods of NH cooling confirming results from previous studies. These reconstructions are tenuous due other factors like advection influencing the isotopic values. More analysis with other proxies should be performed to resolve the precipitation trends in this region.

6. References

Aldrian, E., and R. Dwi Susanto (2003), Identification of three dominant rainfall regions within Indonesia and their relationship to sea surface temperature, *International Journal of Climatology*, *23*(12), 1435-1452.
Anand, P., H. Elderfield, and M. Conte (2003), Calibration of Mg/Ca thermometry in planktonic foraminifera from a sediment trap time series, *Paleoceanography*, *18*(2).
Andreasen, D. H., S. Sosdian, S. Perron-Cashman, C. H. Lear, T. deGaridel-Thoron, P. Field, and Y. Rosenthal (2006), Fidelity of radially viewed ICP-OES and magnetic-sector ICP-MS measurement of Mg/Ca and Sr/Ca ratios in marine biogenic carbonates: Are they trustworthy together?, *Geochemistry Geophysics Geosystems*, *7*(10).
Bard, E., G. Raisbeck, F. Yiou, and J. Jouzel (2000), Solar Irradiance during the last 1200 years based on cosmogenic nuclides, *Tellus*, *52B*, 8.
Beer, J., M. Vonmoos, and R. Muscheler (2006), Solar Variability Over the Past Several Millennia, *Space Science Reviews*, *125*(1-4), 67-79.
Bemis, B. E., and H. J. Spero (1998), Reevaluation of the oxygen isotopic composition of planktonic foraminifera: Experimental results and revised paleotemperature equations, *Paleoceanography*, *13*, 11.
Boyle, E., and L. Keigwin (1987), North Atlantic thermohaline circulation during the past 2,000 years linked to high-latitude surface temperature, *Nature*, *330*, 6.
Broccoli, A. J., K. A. Dahl, and R. J. Stouffer (2006), Response of the ITCZ to Northern Hemisphere cooling, *Geophysical Research Letters*, *33*(1).
Burnett, W., V. Kamenkovich, G. Mellor, and A. Gordon (2000), The influence of pressure head on the Indonesian Seas circulation, *Geophysical Research Letters*, *27*(15), 4.
Cobb, K. M., C. D. Charles, H. Cheng, and L. Edwards (2003), El nino/southern oscillation and tropical Pacific climate during the last millennium, *Nature*, *424*, 6.
Crowley, T. J. (2000), Causes of Climate Change Over the Past 1000 Years, *Science*, *289*(5477), 270-277.
Delworth, T. L., et al. (2006), GFDL's CM2 global coupled climate models. Part I: Formulation and simulation characteristics, *Journal of Climate*, *19*(5), 643-674.
Eddy, J. A. (1976), The Maunder Minimum, *Science*, *192*, 14.
Efron, B. (1982), *The Jacknife, the bootstrap, and other sampling plans*, Standford, CA.
Fairbanks, R. G., R. A. Mortlock, T.-C. Chiu, L. Cao, A. Kaplan, T. P. Guilderson, T. W. Fairbanks, A. L. Bloom, P. M. Grootes, and M.-J. Nadeau (2005), Radiocarbon calibration curve spanning 0 to 50,000 years BP based on paired 230Th/234U/238U and 14C dates on pristine corals, *Quaternary Science Reviews*, *24*(16-17), 1781-1796.
Francey, R., C. Allison, D. Etheridge, C. Trudinger, I. Enting, and M. Leuenberger (1999), A 1,000-year high precision record of c13C in atmospheric CO2, *Tellus*, *51B*, 24.
Gordon, A., R. D. Susanto, and K. Vranes (2003), Cool Indonesian throughflow as a consequence of restricted surface layer flow, *Nature*, *425*(6960), 824-828.

Gordon, A., J. Sprintall, H. M. Van Aken, D. Susanto, S. Wijffels, R. Molcard, A. Ffield, W. Pranowo, and S. Wirasantosa (2010), The Indonesian throughflow during 2004–2006 as observed by the INSTANT program, *Dynamics of Atmospheres and Oceans*, *50*(2), 115-128.
Guilderson, T. P., and D. P. Schrag (1999), Reliability of coral isotope records from the Western Pacific Warm Pool: A comparison using age-optimized records, *Paleoceanography*, *14*(4), 457.
Haug, G. H., K. A. Hughen, D. M. Sigman, L. C. Peterson, and U. Rohl (2001), Southward migration of the intertropical convergence zone through the Holocene, *Science*, *293*(5533), 1304-1308.
Hendy, E. J., M. K. Gagan, C. A. Alibert, M. T. McCulloch, J. M. Lough, and P. J. Isdale (2002), Abrupt decrease in tropical Pacific sea surface salinity at end of Little Ice Age, *Science*, *295*(5559), 1511-1514.
Keeling, R., S. Piper, A. Bollenbacher, and S. Walker (2008), Isotopic ratio of atmospheric 13co2/12co2 (per mil): Station South Pole, edited, Scripps CO2 Program University of California.
Lean, J., J. Beer, and R. Bradley (1995), Reconstruction of solar irradiance since 1610: Implications for climate change, *Geophysical research letters*, *22*, 4.
Linsley, B., Y. Rosenthal, and D. W. Oppo (2010), Holocene evolution of the Indonesian throughflow and the western Pacific warm pool, *Nat Geosci*, *3*(8), 578-583.
Mann, M. E., Z. Zhang, M. K. Hughes, R. S. Bradley, S. K. Miller, S. Rutherford, and F. Ni (2008), Proxy-based reconstructions of hemispheric and global surface temperature variations over the past two millennia, *Proceedings of the National Academy of Sciences of the United States of America*, *105*(36), 13252-13257.
Mann, M. E., Z. Zhang, S. Rutherford, R. S. Bradley, M. K. Hughes, D. Shindell, C. Ammann, G. Faluvegi, and F. Ni (2009), Global signatures and dynamical origins of the Little Ice Age and Medieval Climate Anomaly, *Science*, *326*(5957), 1256-1260.
Mayer, B., P. E. Damm, T. Pohlmann, and S. Rizal (2010), What is driving the ITF? An illumination of the Indonesian throughflow with a numerical nested model system, *Dynamics of Atmospheres and Oceans*, *50*(2), 301-312.
Meyers, G., J. Donguy, and R. Reed (1986), *Evaporative Cooling of the western equatorial Pacific Ocean by anomalous winds*, Nature.
Moberg, A., D. M. Sonechkin, K. Holmgren, N. M. Datsenko, and W. Karlen (2005), Highly variable Northern Hemisphere temperatures reconstructed from low- and high-resolution proxy data, *Nature*, *433*(7026), 613-617.
Mohtadi, M., S. Steinke, J. Groeneveld, H. G. Fink, T. Rixen, D. Hebbeln, B. Donner, and B. Herunadi (2009), Low-latitude control on seasonal and interannual changes in planktonic foraminiferal flux and shell geochemistry off south Java: A sediment trap study, *Paleoceanography*, *24*(1).
Neale, R., and J. Slingo (2003), The Maritime Continent and Its Role in the Global Climate: A GCM Study, *Journal of Climate*, *16*, 15.
Neukom, R., and J. Gergis (2011), Southern Hemisphere high-resolution palaeoclimate records of the last 2000 years, *The Holocene*, *22*(5), 501-524.

Newton, A., R. Thunell, and L. Stott (2006), Climate and hydrographic variability in the Indo-Pacific Warm Pool during the last millennium, *Geophysical Research Letters*, *33*(19).
Newton, A., R. Thunell, and L. Stott (2011), Changes in the Indonesian Throughflow during the past 2000 yr, *Geology*, *39*(1), 63-66.
Nurhati, I. S., K. M. Cobb, and E. Di Lorenzo (2011), Decadal-Scale SST and Salinity Variations in the Central Tropical Pacific: Signatures of Natural and Anthropogenic Climate Change, *Journal of Climate*, *24*(13), 3294-3308.
Oppo, D. W., Y. Rosenthal, and B. K. Linsley (2009), 2,000-year-long temperature and hydrology reconstructions from the Indo-Pacific warm pool, *Nature*, *460*(7259), 1113-1116.
Qu, T., H. Yan, J. Strachan, G. Meyers, and J. Slingo (2005), Sea Surface Temperature and its variability in the Indonesian egion, *Oceanography*, *18*, 12.
Rosenthal, Y., E. Boyle, and N. Slowey (1997), Temperature control on te incorporation of magnesium, strontium, fluorine, and cadium into benthic foraminferal shells from Little Bahama Bank: Prospects for thermocline paleoceanography, *Geochimica et Cosmochimica Acta.*, *61*(17), 11.
Rosenthal, Y., M. Field, and R. Sherrell (1999), Precise Determination of Element/ Calcium Ratios in Calcareous Samples Using Sector Field Inductively Coupled Plasma Mass Spectrometry, *Analytical Chemistry*, *71*, 6.
Sachs, J. P., D. Sachse, R. H. Smittenberg, Z. Zhang, D. S. Battisti, and S. Golubic (2009), Southward movement of the Pacific intertropical convergence zone AD 1400–1850, *Nat Geosci*, *2*(7), 519-525.
Smith, T. M., W. Richard, L. C. Peterson, and J. Lawrimore (2008), Improvements to NOAA'S Historical Merged Land-Ocean Surface Temperature Analysis (1880-2006), *Journal of Climate*, *21*, 48.
Steinhilber, F., J. Beer, and C. Fröhlich (2009), Total solar irradiance during the Holocene, *Geophysical Research Letters*, *36*(19).
Stothers, R. (1984), The great Tambora eruption in 1815 and its aftermath, *Science*, *224*.
Swart, P. K., L. Greer, B. E. Rosenheim, C. S. Moses, A. J. Waite, A. Winter, R. E. Dodge, and K. Helmle (2010), The13C Suess effect in scleractinian corals mirror changes in the anthropogenic CO2inventory of the surface oceans, *Geophysical Research Letters*, *37*(5).
Tierney, J. E., D. W. Oppo, Y. Rosenthal, J. M. Russell, and B. K. Linsley (2010), Coordinated hydrological regimes in the Indo-Pacific region during the past two millennia, *Paleoceanography*, *25*.
Wang, Y. J., H. Cheng, R. L. Edwards, Y. Q. He, X. G. Kong, Z. S. An, J. Y. Wu, M. J. Kelly, C. A. Dykoski, and X. D. Li (2005), The Holocene Asian monsoon: Links to solar changes and North Atlantic climate, *Science*, *308*(5723), 854-857.
Wanner, H., et al. (2008), Mid- to Late Holocene climate change: an overview, *Quaternary Science Reviews*, *27*(19-20), 1791-1828.
Wilson, R., A. Tudhope, P. Brohan, K. Briffa, T. Osborn, and S. Tett (2006), Two-hundred-fifty years of reconstructed and modeled tropical temperatures, *Journal of Geophysical Research*, *111*(C10).

Wyrtki, K. (1961), Physical Oceanography of Southeast Asian waters., *Naga Report 2. Scripps Institution of Oceanography*.
Wyrtki, K. (1987), Indonesia Through Flow and Associated Pressure Gradient, *Journal of Geophysical Research*, *92*, 6.
Xie, P., and P. Arkin (1996), Analyses of Global Monthly Precipitation Using Guage Observations, Satellite Estimates, and numerical Model Predictions, *Journal of Climate*, *9*, 19.
Yan, X.-H., C.-R. Ho, Q. Zheng, and V. Klemas (1992), Temperature and Size Variabilities of the Western Pacific Warm Pool, *Science*, *258*(5088), 1643-1645.
Yancheva, G., N. R. Nowaczyk, J. Mingram, P. Dulski, G. Schettler, J. F. Negendank, J. Liu, D. M. Sigman, L. C. Peterson, and G. H. Haug (2007), Influence of the intertropical convergence zone on the East Asian monsoon, *Nature*, *445*(7123), 74-77.
Zhang, P., H. Cheng, L. Edwards, and F. Chen (2008), A test of Climate, Sun, and Culture Relationships from an 1810-Year Chinese Cave Record, *Science*, *322*, 3.
Zhang, Y., J. M. Wallace, and D. Batisti (1997), ENSO-like interdecadal variability: 1900-93, *Journal of climate*, *10*, 17.
Zielinski, G. (2000), Use of paleo-records in determining variability within the volcanism-climate system, *Quaternary Science Reviews*, *19*.

7. Tables

Table 1. Core Locations. The locations of the cores analyzed in this study.

Core Name (GGC & MC)	Short Name	Latitude	Longitude	Water Depth(m)
BJ8-03 85 GGC/ BJ8-03 84 MC	BJ-85	-1 23.914	117 31.295	403
BJ8-03 7 GGC/ BJ8-03 6 MC	BJ-7	-7 28.659	115 21.186	909
BJ8-03 142 MC	BJ-142	-8 28.314	117 51.093	296

Table 2. Radiocarbon Dates. All measurements are made at the National Ocean Sciences Accelerator Mass Spectrometry Facility (NOSAMS) on mixed planktonic foraminifera and converted to calendar age using a reservoir age of 500 years.

Core	NOSAMS ID	Depth (cm)	14C Age ± 1 s	Calendar Age ± 1 s (BP)	Foraminifera
7GGC	88959	12-14	445 ± 30	>Modern	G. ruber, P. obliquilata, G. sacculifer
7GGC	78915	50-52	1293 ± 20	702 ± 16	G. ruber, G. sacculifer
7GGC	88960	163-164	2210 ± 35	1611 ± 50	G. ruber, P. obliquilata, G. sacculifer
7GGC	78916	200-202	2867 ± 20	2355 ± 16	G. ruber, G sacculifer
7GGC	78917	350-352	4323 ± 20	4212 ± 37	G. ruber, G. sacculifer
7GGC	88961	448-449	5781 ± 40	6038 ± 69	G. ruber, P. obliquilata, G. sacculifer
MC6	88958	43-44	745 ± 30	286 ± 53	G. ruber, P. obliquilata, G. sacculifer
85GGC		1-2	90 ± 25	>Modern	G. ruber, G. sacculifer
85GGC	107431	49.5-52.5	1130 ± 25	528 ± 33	G. ruber, G. sacculifer
85GGC	107432	99.5-102.5	1670 ± 30	1076 ± 42	G. ruber, G. sacculifer
85GGC	107433	171.5-172.5	2230 ± 30	1730 ± 59	G. ruber , G. sacculifer
85GGC		354-355	4850 ± 35	4891 ± 47	G. sacculifer
MC84 B		0-1	>Modern	>Modern	G. ruber, G. sacculifer
MC84 B		54-55.5	815 ± 30	370 ± 54	G. sacculifer

Table 3. Lead Isotopes. Samples are analyzed at WHOI.

Core	Avg Depth (cm)	Excess ^{210}Pb (dpm/gdw)	Count error (dpm/gdw)	Age (CE)
BJ-142	0	23.41	0.61	2003
BJ-146	4	22.87	0.69	2002.2
BJ- 142	6	19.18	0.64	1996.6
BJ 146	9	14.37	0.53	1987.3
BJ-142	11	9.36	0.37	1973.5
BJ-146	14	5.69	0.32	1957.5

Table 4. Ash Layers. Below are the depths where ash layers were detected from percent coarse fraction (>20%) and also, for the gravity core, in the magnetic susceptibility.

Core	Depth (cm)	Eruption	Year (CE)
BJ-142	47	Mt. Tambora	1815
BJ-6	25.5	Mt. Tambora	1815
BJ-7	15.5	Mt. Tambora	1815

Table 5. CM2.1 Locations. The locations where CM2.1 model data are extracted.

Representative of Core	Latitude	Longitude
MD-77	2	119
BJ-85	-1	118
BJ-34	-4	119
MD-60	-5	118
BJ-7	-8	115

8. Figures

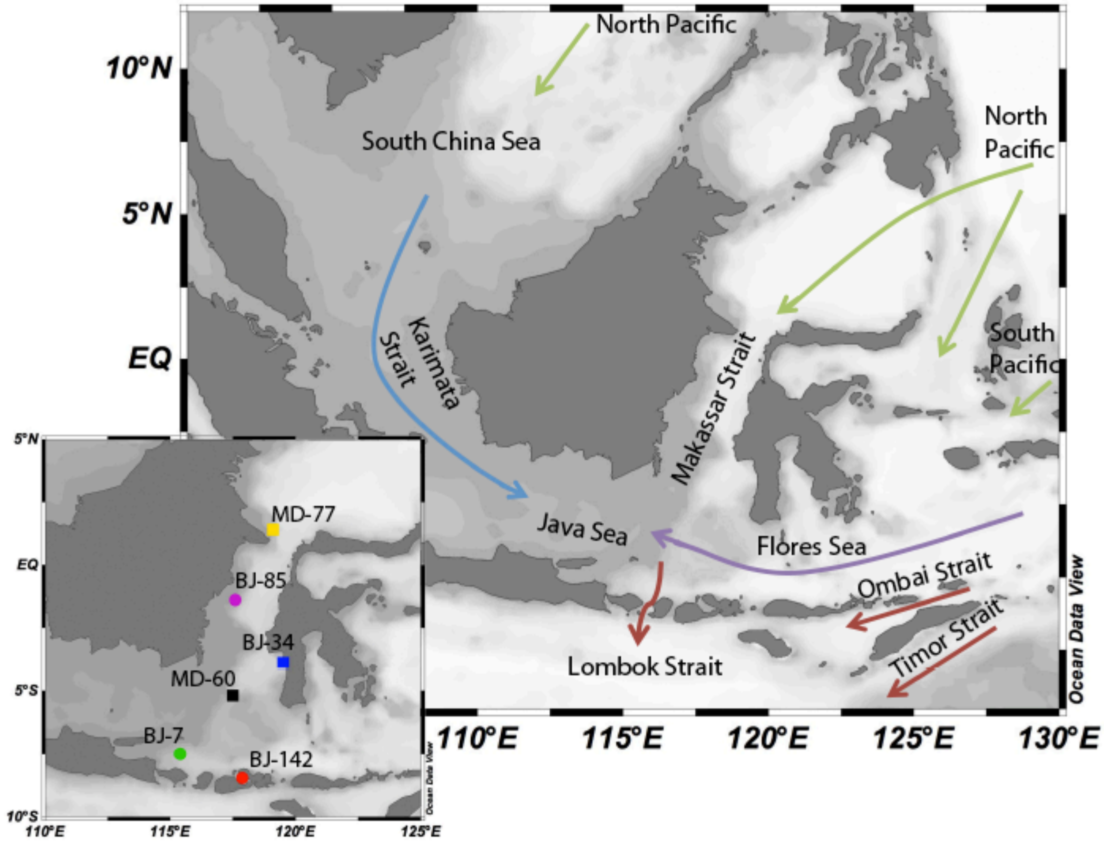

Figure 1. Surface currents and sites of proxy records. The primary inflow and outflow portals of the ITF are shown by green and red arrows, respectively. The blue arrow represents the flow during the Indonesian boreal winter monsoon and the purple during the Indonesia boreal summer monsoon. The insert is a scaled up depiction of cores location in the Makassar Strait and the Java Sea; additional information for each core site is located in table 1. The sites indicated with a square (yellow, MD-77; blue, BJ-34; black, MD-60) are from previous studies [*Newton et al.*, 2011; *Oppo et al.*, 2009] whereas the circles (purple, BJ-85; green, BJ-7) represent data from this study.

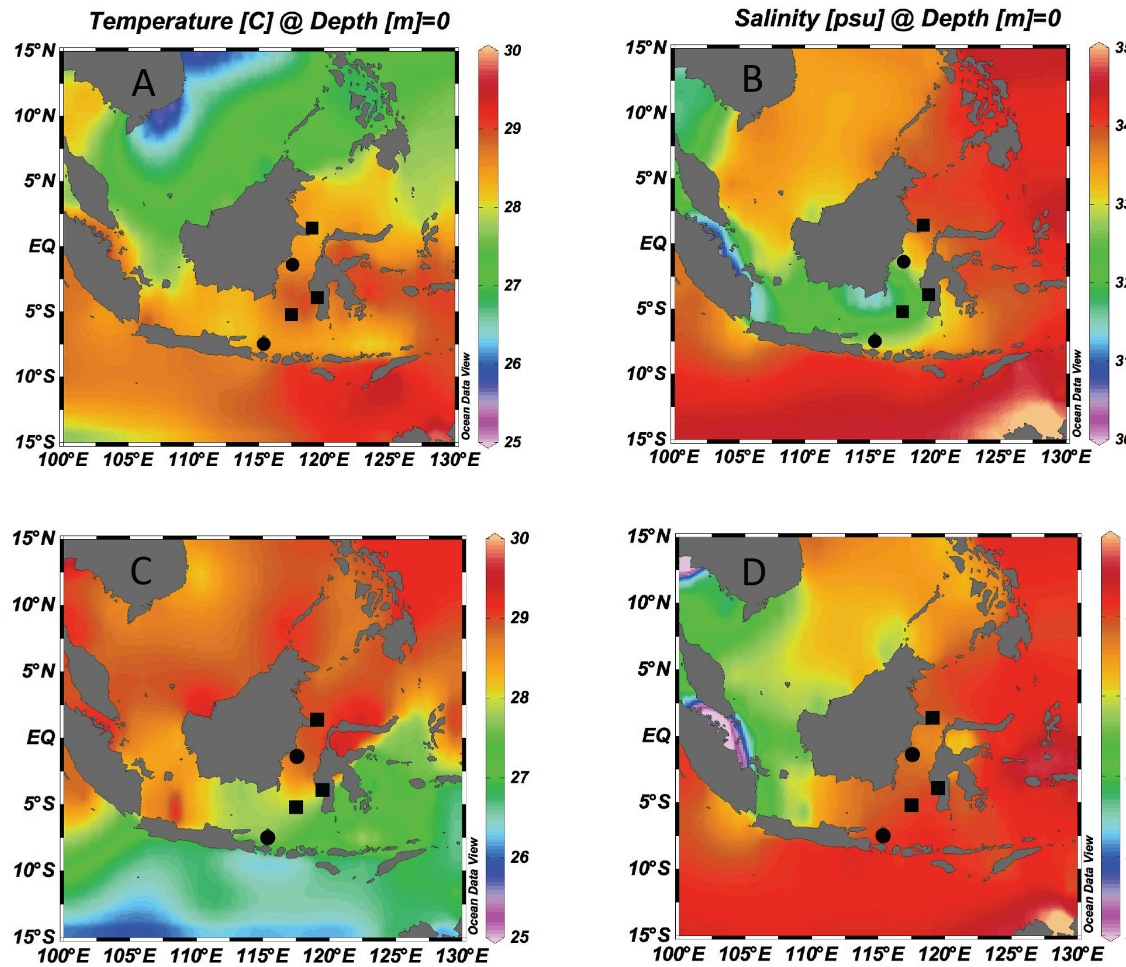

Figure 2. Instrumental climate averages. A) January-March (JFM) averaged SST, B) JFM averaged salinity, C) July- September (JAS) SST and D) JAS averaged salinity. All plots are from Ocean Data View using World Ocean Atlas 2009 compiled and smoothed ship and bouy data from stations that are 1x1 degrees apart. The black squares are the locations of published *G. ruber* SST records [*Newton et al.*, 2011; *Oppo et al.*, 2009] whereas the black circles are the two new records from this study (See section 3.1).

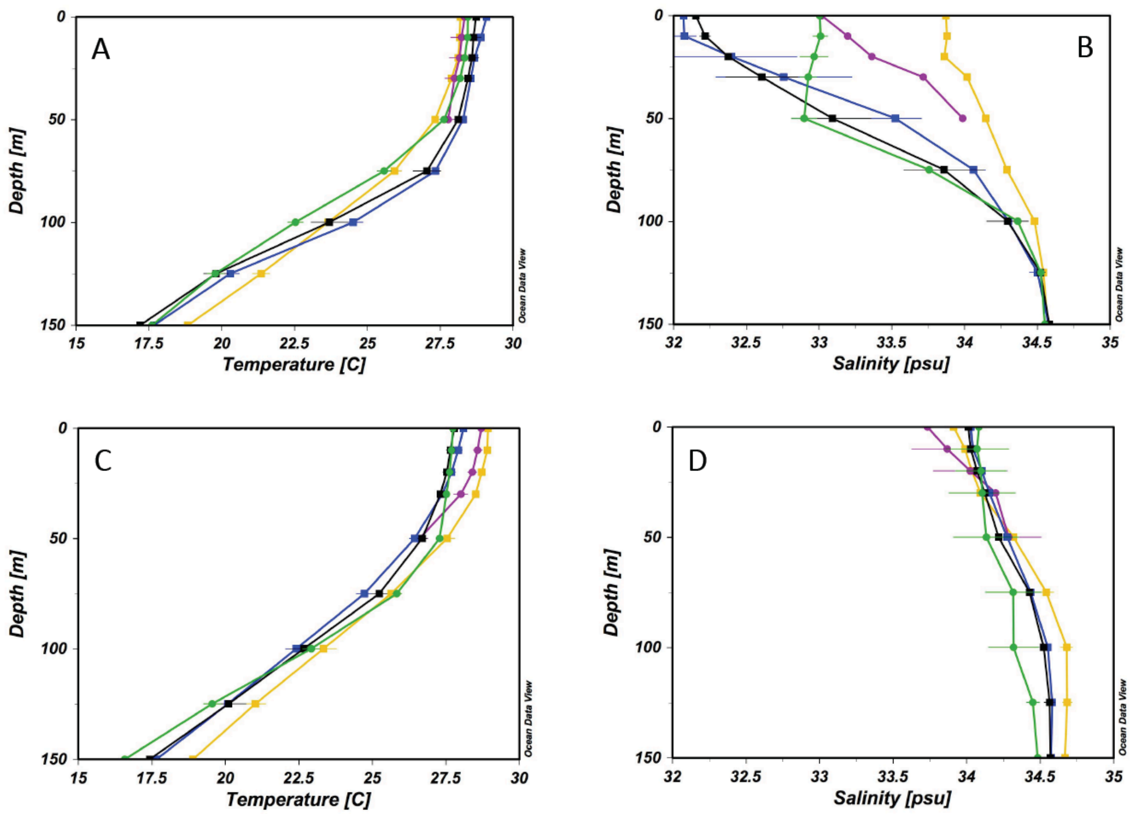

Figure 3. Depth profiles. A) Temperature in JFM, B) Salinity in JFM, C) Temperature in JAS, D) Salinity in JAS, where yellow refers to site MD-77, purple BJ-85, blue BJ-34, black MD-60 and green BJ-7. All plots are from Ocean Data View using World Ocean Atlas 2009 compiled ship and buoy data at stations near each core site.

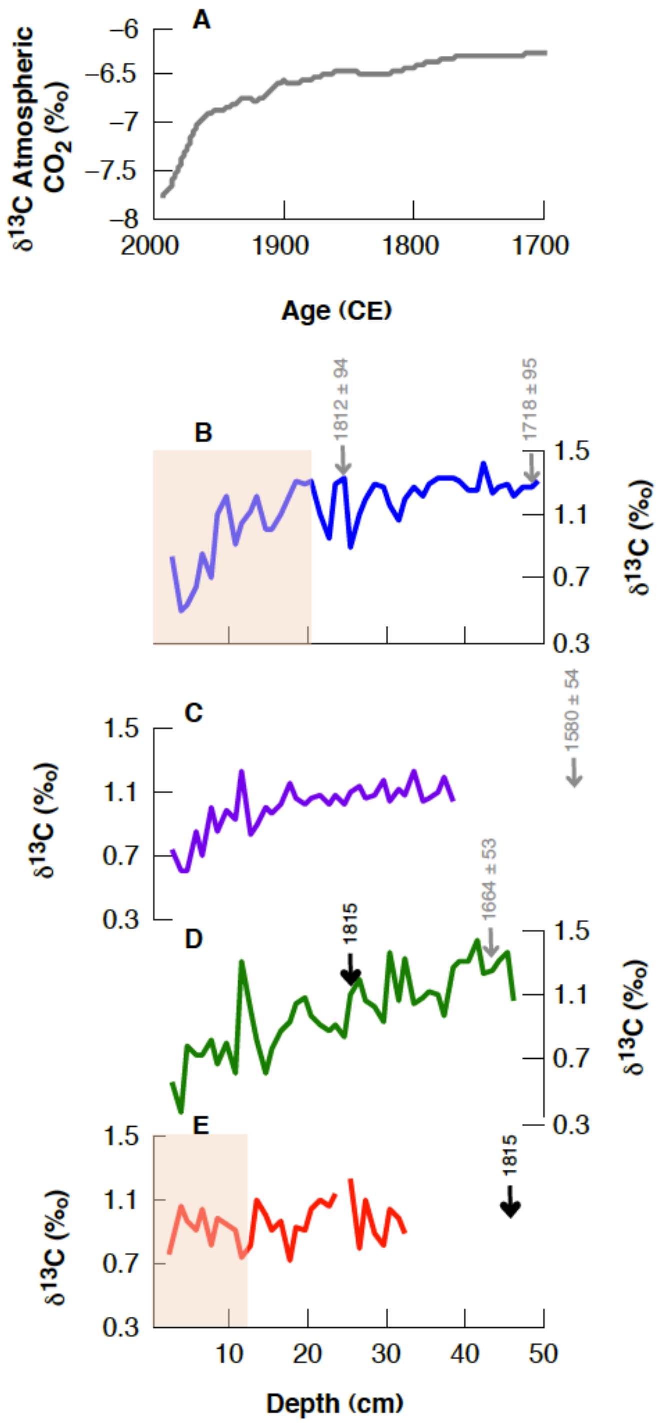

Figure 4. Age model tools. Compared above are the raw $\delta^{13}C$ values from the multi-cores (B-E) with the reconstructed carbon isotopic values of atmospheric CO_2 demonstrating the Suess effect (A) [*Francey et al.*, 1999]. The decline of $\delta^{13}C$ from the multi-cores is correlated with this reconstruction. The grey arrows show where ^{14}C dates were collected and are converted to calendar age (CE) with the one-sigma standard deviation. The black arrows indicate the depth where Mt. Tambora ash layer is found. Finally the shaded pink area is where ^{210}Pb isotopes are run. A) Francey et al (1999) carbon isotope CO_2 atmospheric reconstruction, B) the blue curve is BJ-31 [*Oppo et al.*, 2009] followed by, C) BJ-84 in purple, D) BJ-6 in green and E) BJ-142 in red from this study.

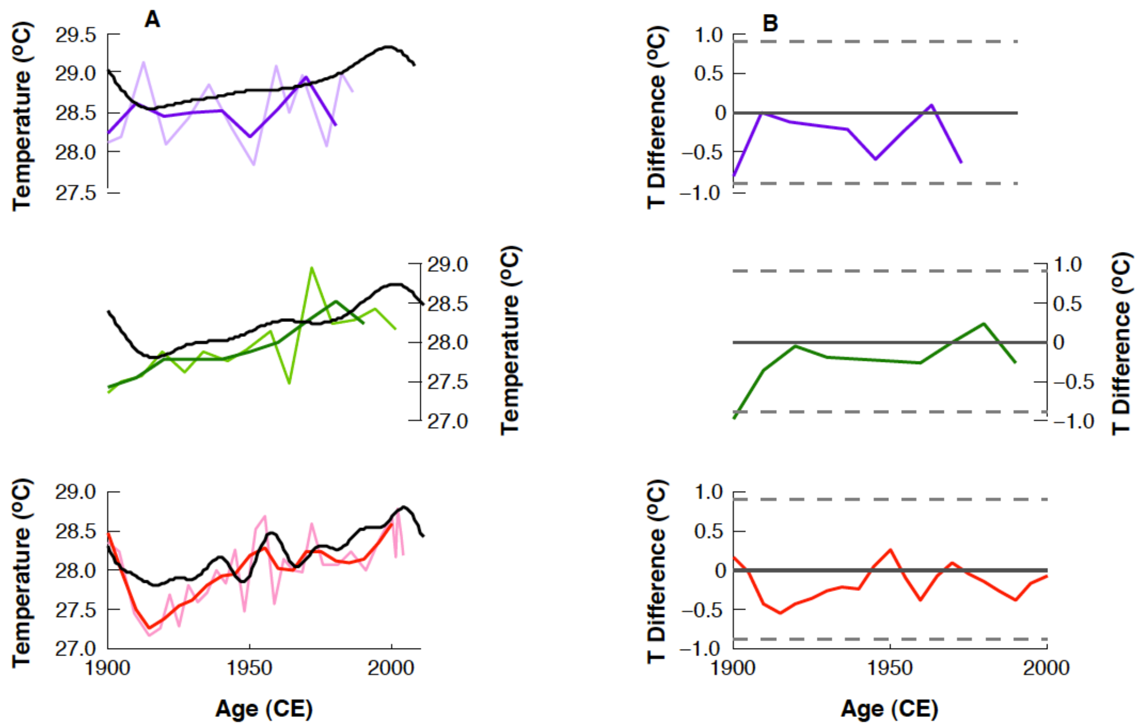

Figure 5. Calibration validation. Plot (A) is the Mg/Ca derived SST from the three multi-cores starting with purple BJ-84, green BJ-6 and red BJ-142. The light colored line marks the raw data whereas the dark colored line is with a 30 yr low pass filter for BJ-84 and BJ-6, where BJ-142 has a 15 yr smoothing filter. On top of each of these SST reconstructions in black is the ERSSTv3 smoothed the same way as the proxy data [*Smith et al.*, 2008]. The plots on right (B) show the difference between the smoothed proxy derived SST and smoothed ERSSTv3 records with the one-sigma standard error marked by the grey dashed lines (see methods 3.7).

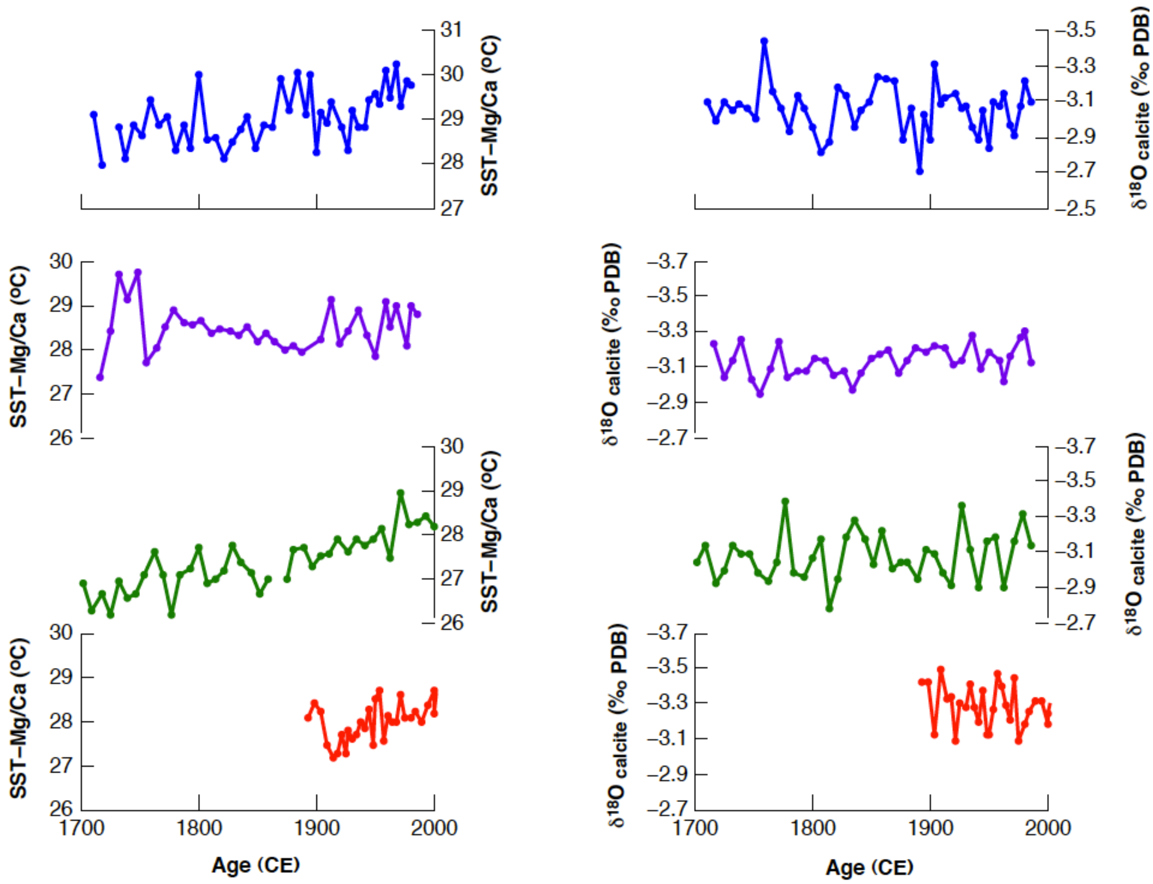

Figure 6A. Raw data for multi-cores. Shown above are the raw data from the published multi-core BJ-31 (blue; Oppo et al 2009) followed by the multi-cores in this study BJ-84 purple, BJ-6 green, BJ-142 red. The figures on the left are the magnesium calcium (Mg/Ca) derived SST, followed by the oxygen isotopes in parts per mil. (See section 3.2 for more details on methods). Note that all records, except BJ-6 suggests significant SST warming over the past century.

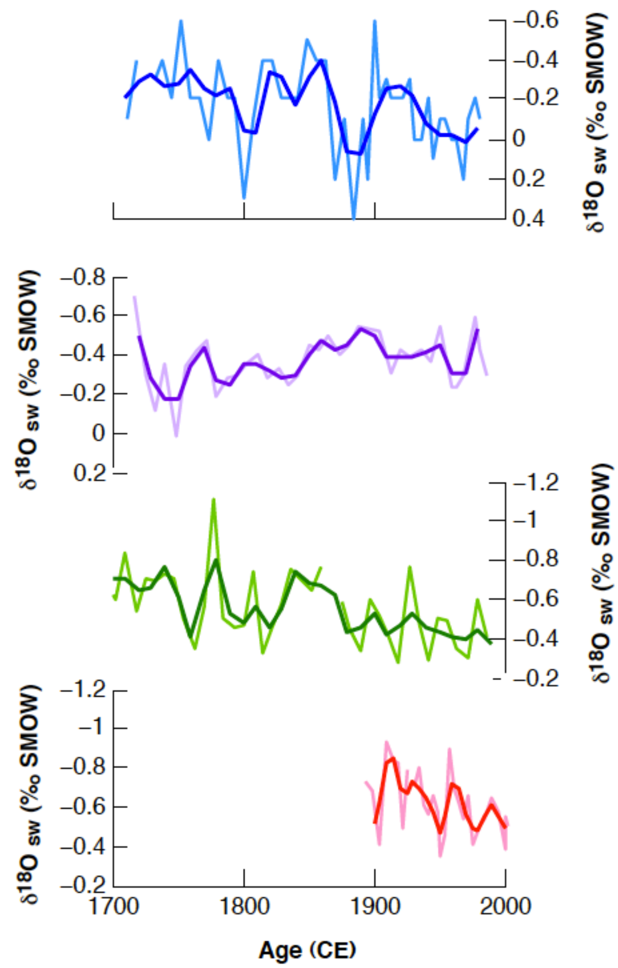

Figure 6B. Reconstructed $\delta^{18}O_{sw}$. Shown above are the reconstructed $\delta^{18}O_{sw}$ values for the multi-cores where blue is BJ-31[*Oppo et al.*, 2009], purple is BJ-84, green BJ-6 and red BJ-142. More enriched values refer to drier conditions or more "saline". The light line is the raw $\delta^{18}O_{sw}$ values and the dark line with a 30 yr low pass filter for all except BJ-142 where a 15 yr low pass filter is used.

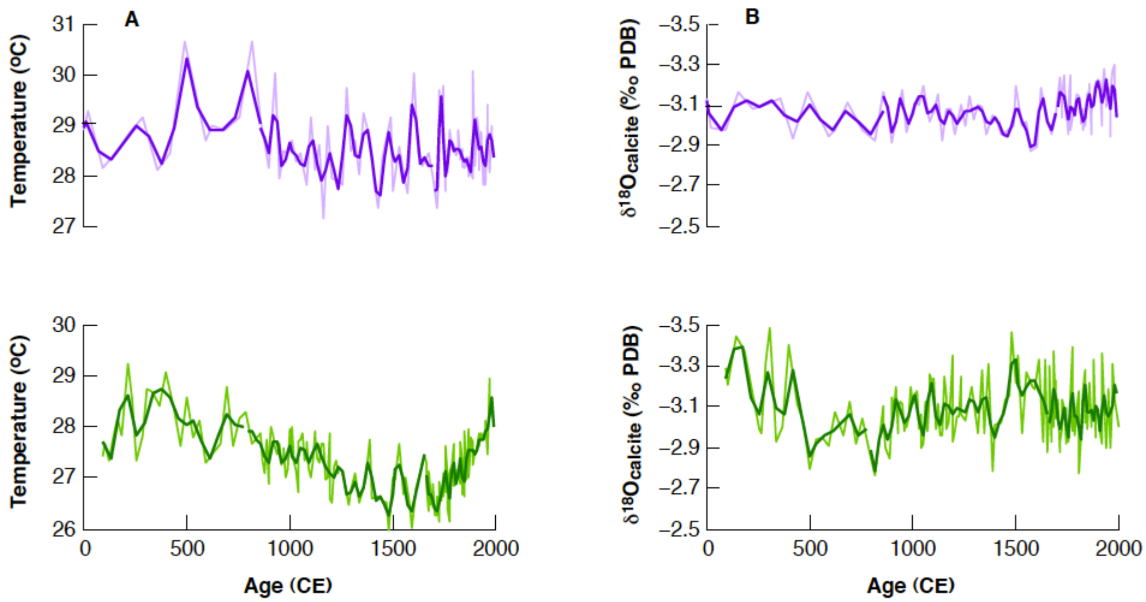

Figure 7. Common Era records. In both plots A and B purple represents combined multi-gravity cores at site BJ-85 and green corresponds to both multi-gravity cores at site BJ-7. Plot A is showing the Mg/Ca derived SST where plot B displays the $\delta^{18}O_{calcite}$ measurements (See methods section 3.2.2).

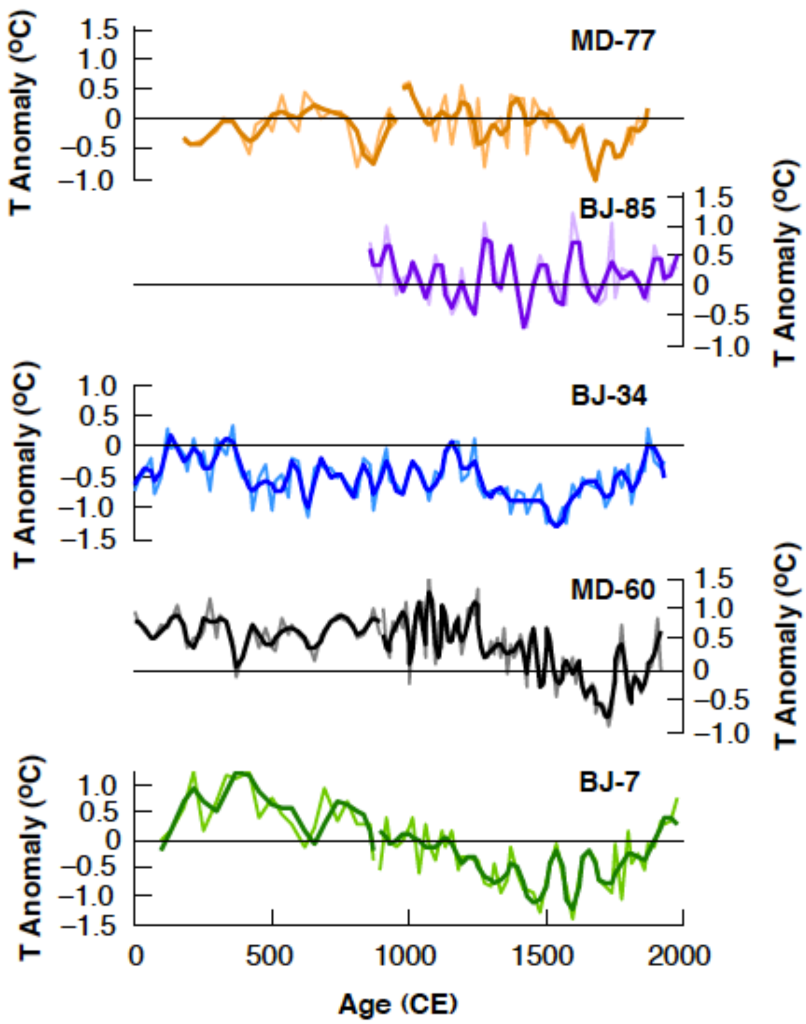

Figure 8. Anomalies all sites. Temperature anomaly records from each site in the Makassar Strait: orange MD-77 [*Newton et al.*, 2011]; purple BJ-85 (this study); blue BJ-34 [*Oppo et al.*, 2009]; black MD-60 [*Newton et al.*, 2011]; green BJ-7 (this study). The light lines are the interpolated data, when the data has been converted into even time steps using the lowest resolution as the time interval. The dark lines are when a low pass filter has been applied using 4 data points from the interpolated data set (See methods section 3.5).

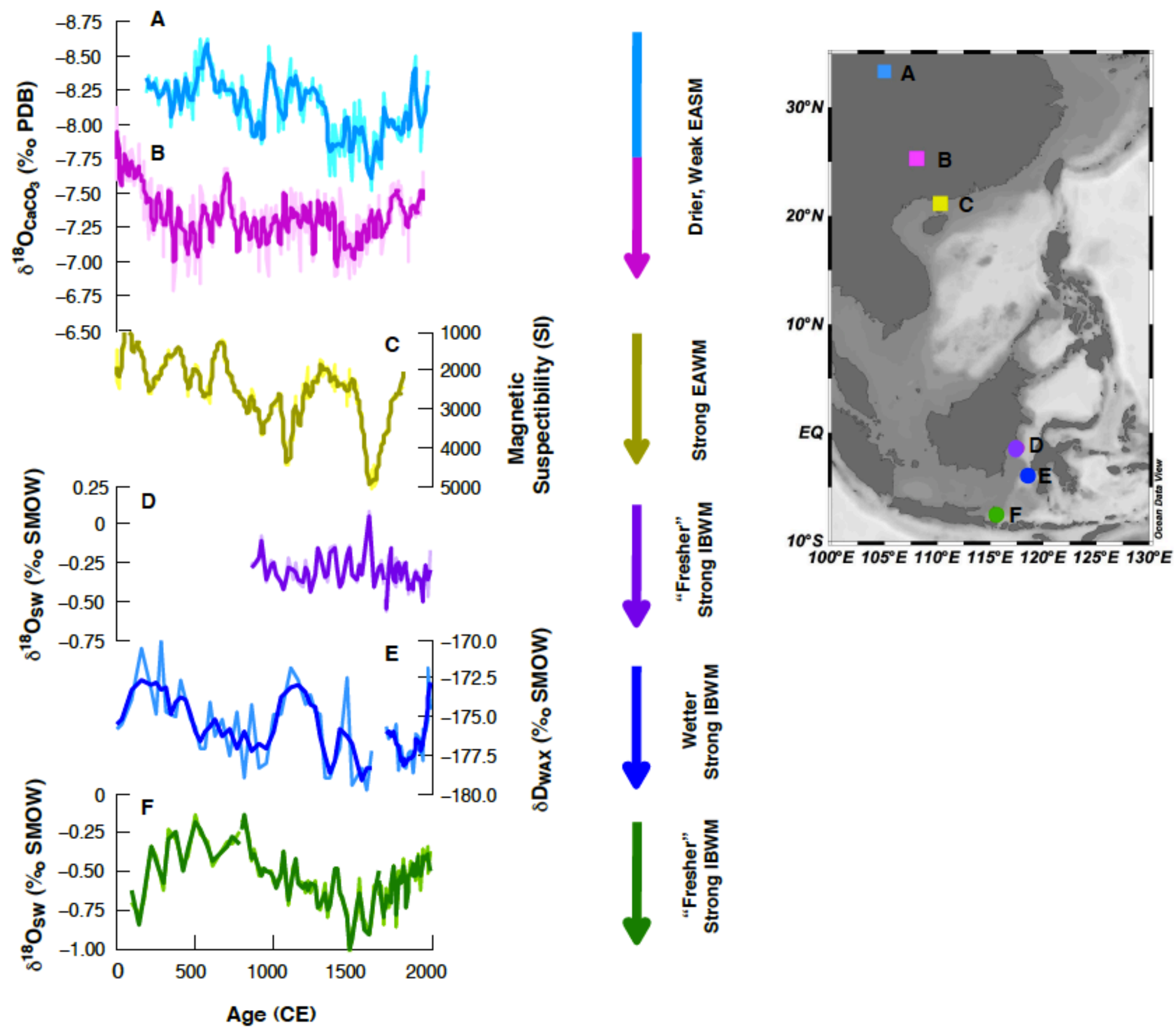

Figure 9. ITCZ Migrations. A) $\delta^{18}O_{CaCO3}$ record from a speleothem in Wanxiang Cave China where more enriched values are drier conditions suggestive of weaker East Asian summer monsoon (EASM) [*P Zhang et al.*, 2008]. This record is evenly interpolated to 15 year time steps shown in light blue and smoothed to 45 years shown in dark blue. B) $\delta^{18}O_{CaCO3}$ record (pink) from a speleothem in Dongge Cave with same interpretation as A [*Wang et al.*, 2005]. C) Magnetic susceptibility on sediments in Lake Huguang Maar where higher values correspond to stronger East Asain winter monsoon (EAWM) [*Yancheva et al.*, 2007]. Both B and C are evenly interpolated to 5 year times steps shown in light colored lines and smoothed to 40 years shown by the darker lines. D) $\delta^{18}O_{sw}$ of sea water reconstruction from site BJ-85 (this study) where more depleted values refer to "fresher" conditions (see methods 3.2.2). E) δD_{wax} record on leaf waxes from sediments in cores BJ-31 and BJ-34 where more depleted values represent wetter conditions and a strengthen Indonesian boreal winter monsoon (IBWM) [*Tierney et al.*, 2010]. The raw data are shown in light blue whereas the 3 point moving average is in dark blue [*Tierney et al.*, 2010]. F) $\delta^{18}O_{sw}$ of sea water reconstruction from site BJ-7 (this study) where more depleted values refer to "fresher" conditions. Both D and F are smoothed to 80 years from 2000-800 CE and then BJ-7 is smoothed to 120 years.

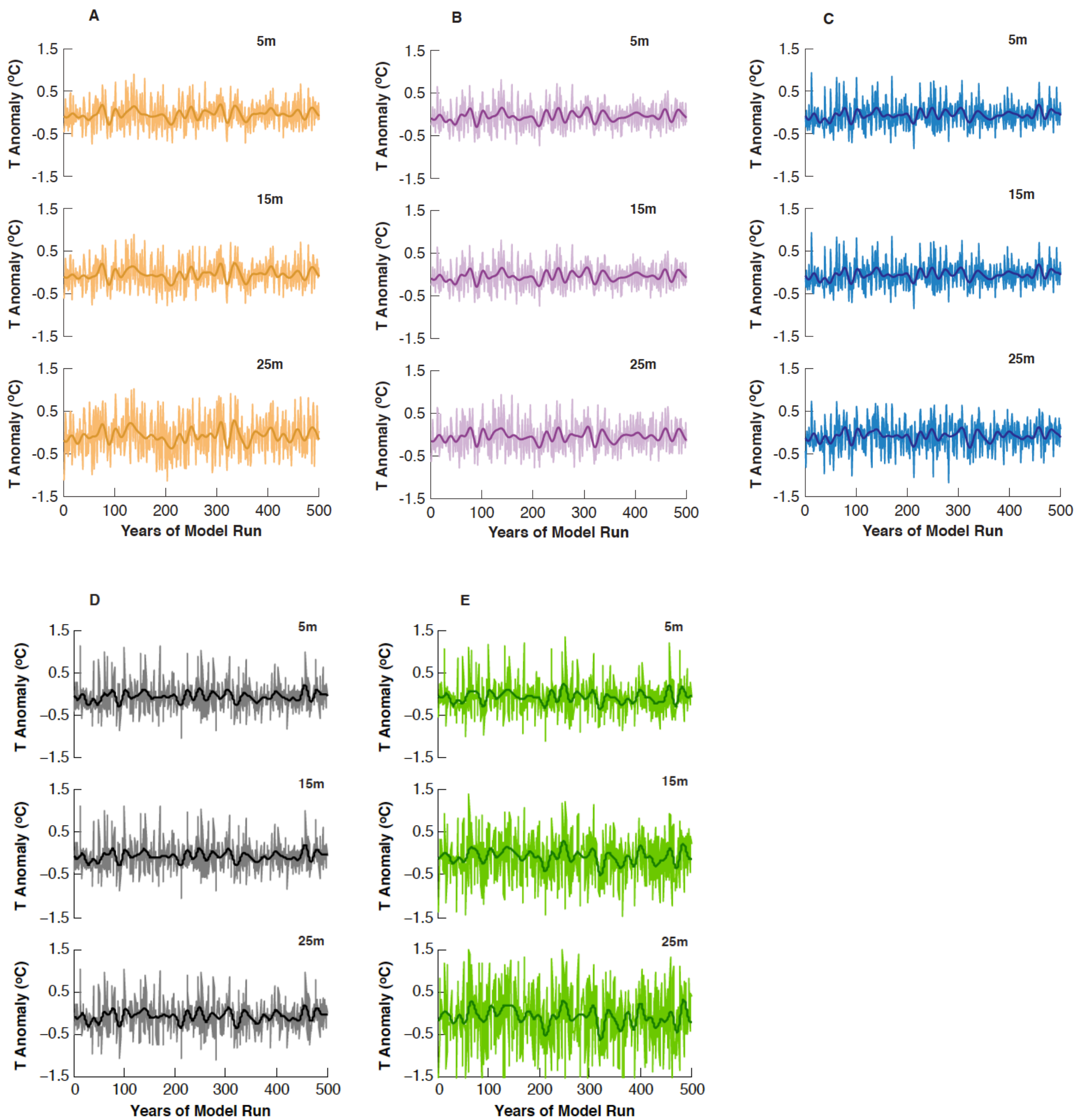

Figure 10. Model Results. Shown above are the SST anomalies from the CM2.1 unforced model experiment at the location of each core site for three depths 5m, 15m, and 25m (see methods 3.6). Figure A) or orange represents site MD-77, B) purple represents BJ-85, C) blue represents BJ-34, D) black represents MD-60 and E) green represents BJ-7.

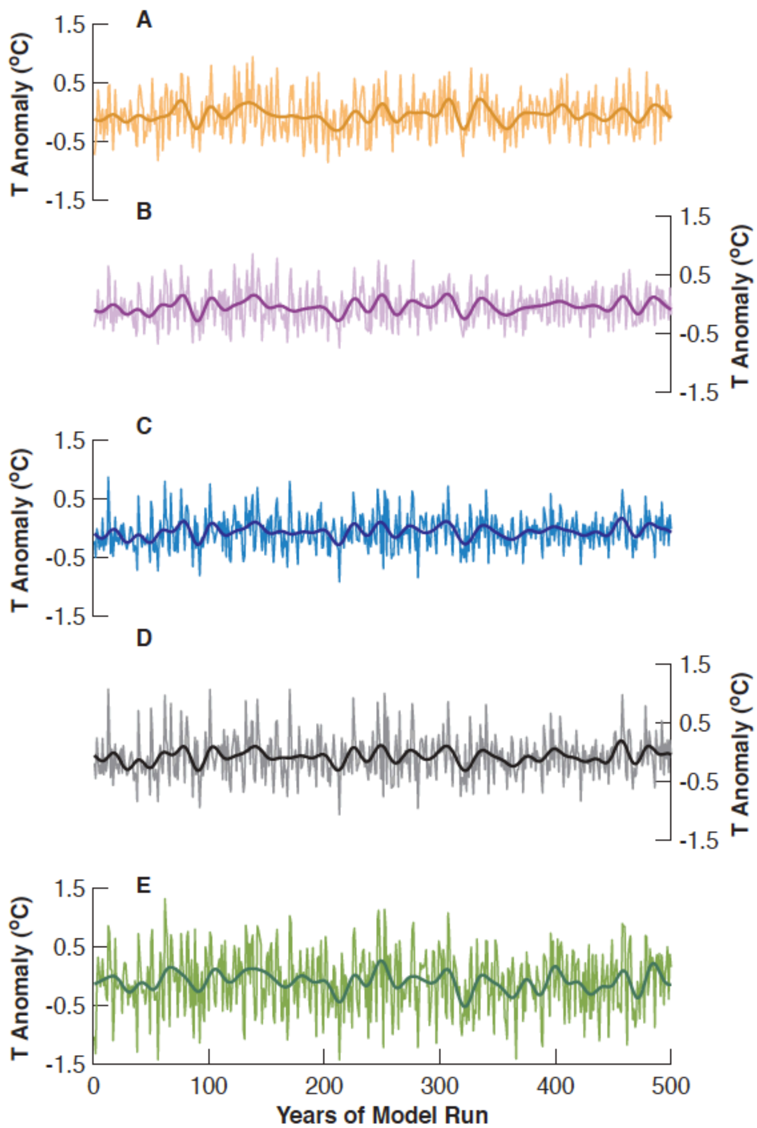

Figure 11. Model results depth averaged. Shown above are the annual SST anomalies averaged from depths 5-25m (Fig. 10) where the light line is the depth-averaged data while the dark line is smoothed to 20 yrs (See methods 3.6). A) orange represents site MD-77, B) purple represents BJ-85, C) blue represents BJ-34, D) green represents BJ-7 and E) black represents MD-60.

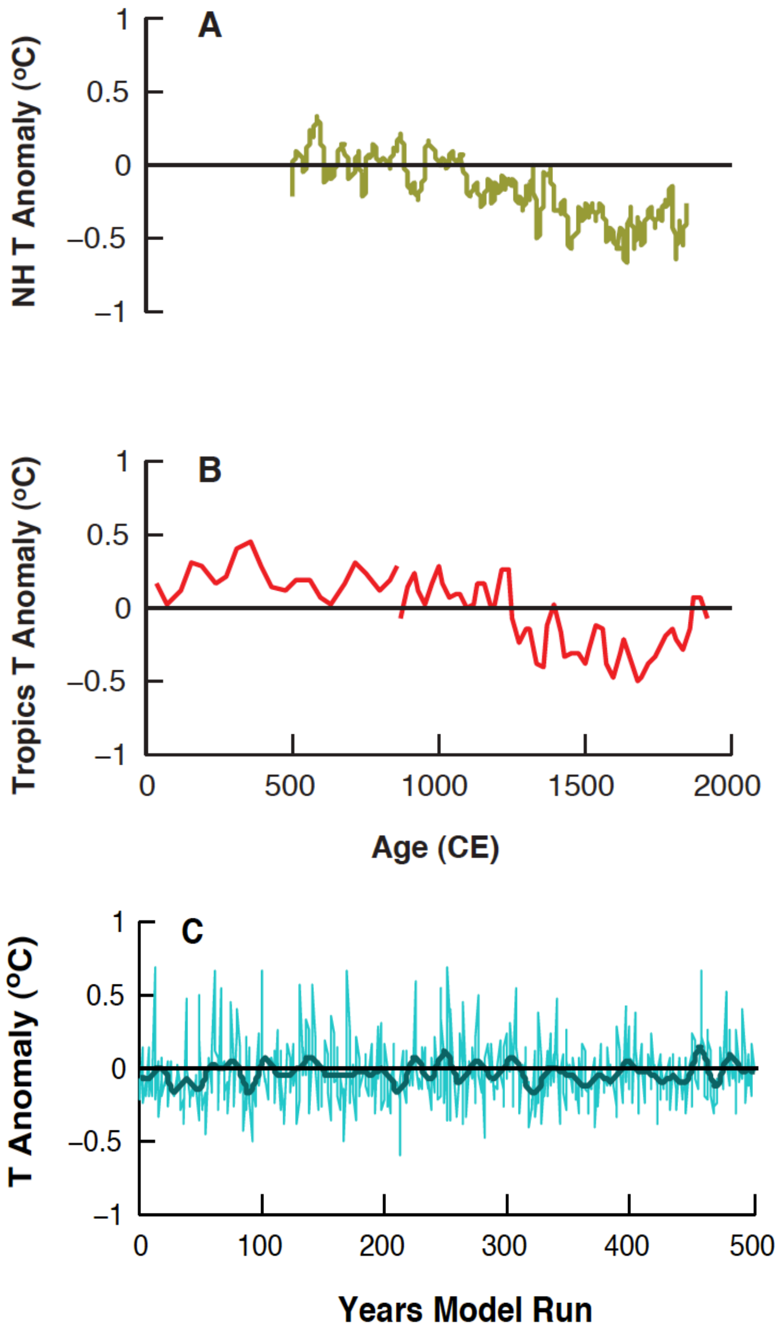

Figure 12. Compilations. A) Shown in green is the *Mann et al.* [2008] NH temperature reconstruction smoothed to 20 years where the reference period is 1961-1990 CE. B) Below that in red is the SST compilation of all the proxy records from the Makassar Strait and Java Sea (MD-77, BJ-85, BJ-34, MD-60 and BJ-7; see section 3.5) where the reference period is from 1860-1890 CE. From 2000-800 CE the proxy compilation is smoothed to 80 yrs and for the rest of the record smoothed to 160 years. C) In teal is the compilation of model data from CM2.1 performed in the same way as the proxy data in (B) from 5-25 m (see methods 3.6) where the light line is the raw data and the dark line is smoothed to 20 years. The reference period used to calculate temperature anomalies was 470-500 model years, but since a model result and not reflecting a particular time any period of 30 years could be used.

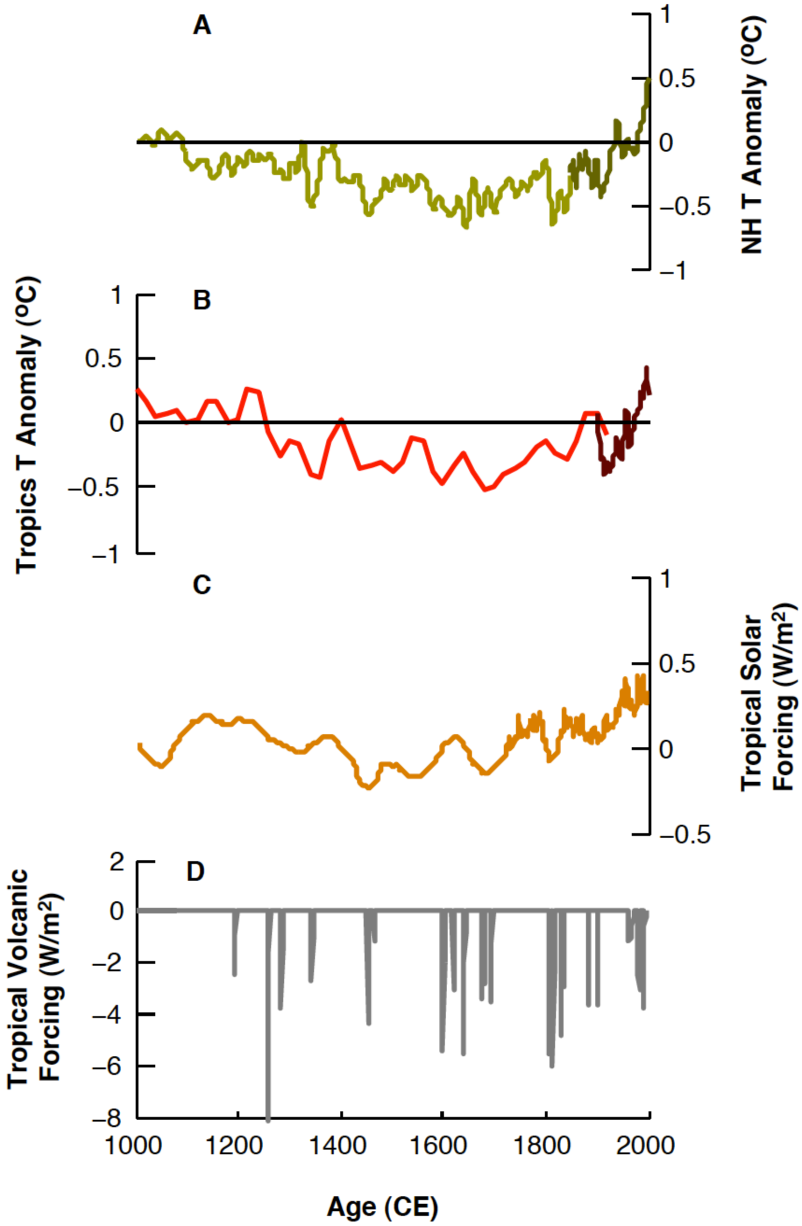

Figure 13. LIA forcings. A) Shown in green is the *Mann et al.* [2009] NH compilation with their compiled instrumental record in dark green. B) The red curve is the SST compilation of the proxy records from this study while the dark red is the averaged compiled ERSSTv3 from the core sites with the reference period of 1860-1890 CE. C & D) Mann et al 2005 compilation of solar forcings and volcanic forcings, respectively in the tropics.

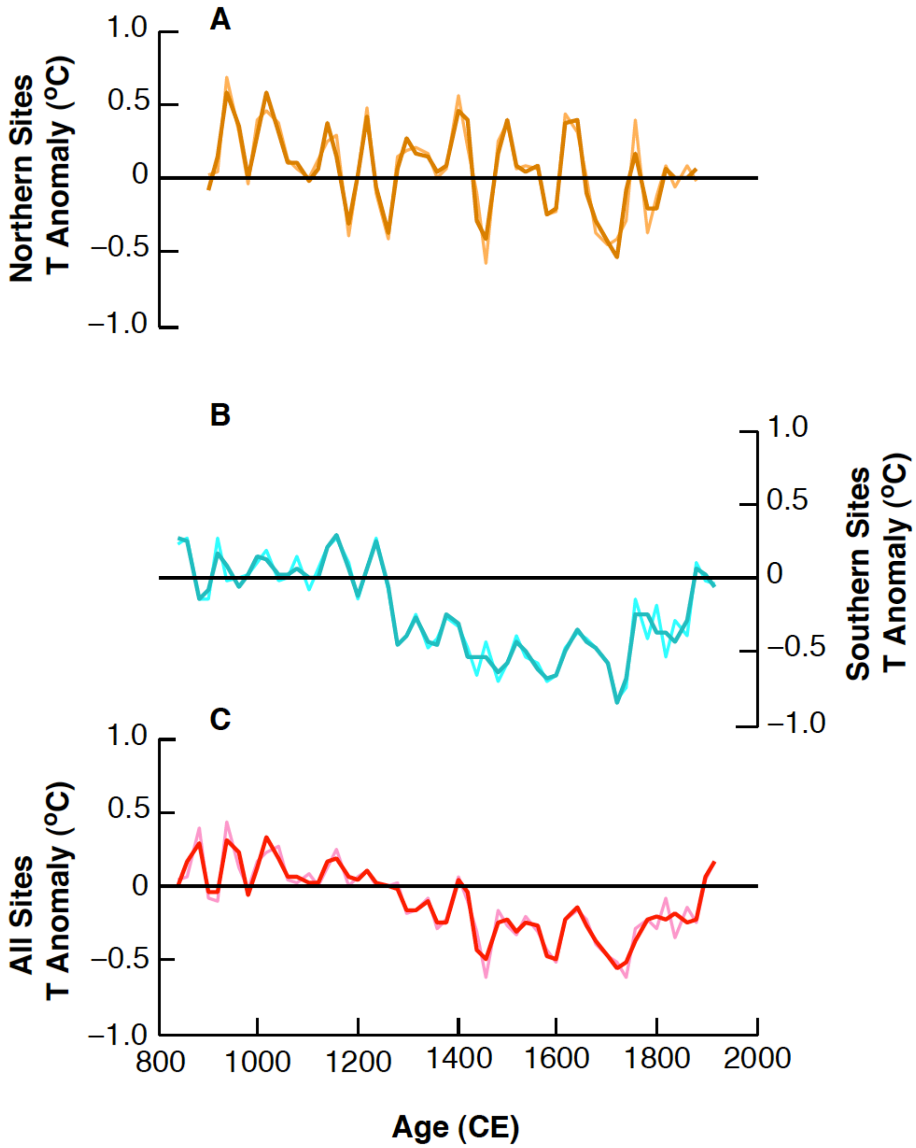

Figure 14. Compilations of northern and southern records. A) Shown in orange is the compilation using only sites BJ-85 and MD-77. B) In teal is the compilation using all the Southern sites, BJ-34, MD-60 and BJ-7. C) In red is the compilation with all five sites. For each compilation the light line is the compilation interpolated to even time steps of 20 years where the dark line is when the compilation has been smoothed to 60 years. Note the strong multi-decadal variability characterizing the northern sites which is absent from the southern records, which likely suggest a strong local influence on the former sites.

9. Appendix

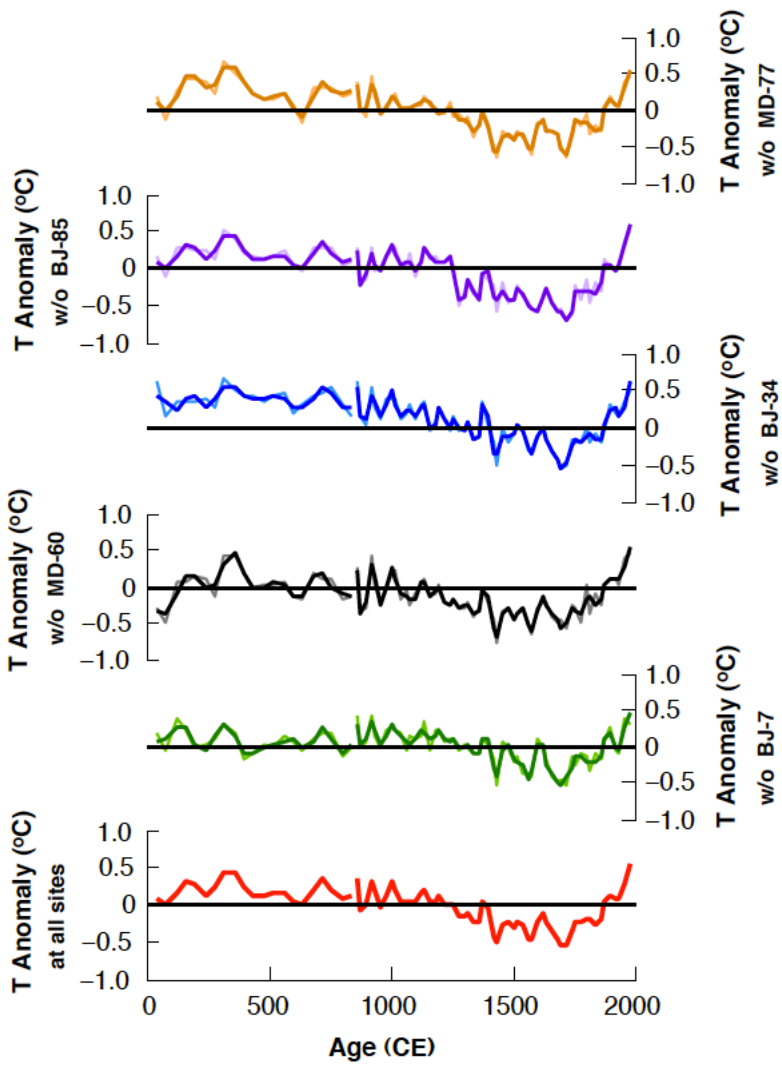

Figure Apx1. Jacknife Approach. Shown above is the compilation from Figure 12 performed five times omitting one record each time [*Efron*, 1982]. The first five compilations are performed by using all the records except the following; yellow all except MD-77, purple all the records except BJ-85, blue all except BJ-34, black all except MD-60, and green all except BJ-7 (See methods section 3.7). The red curve is the compilation using all five proxy records.

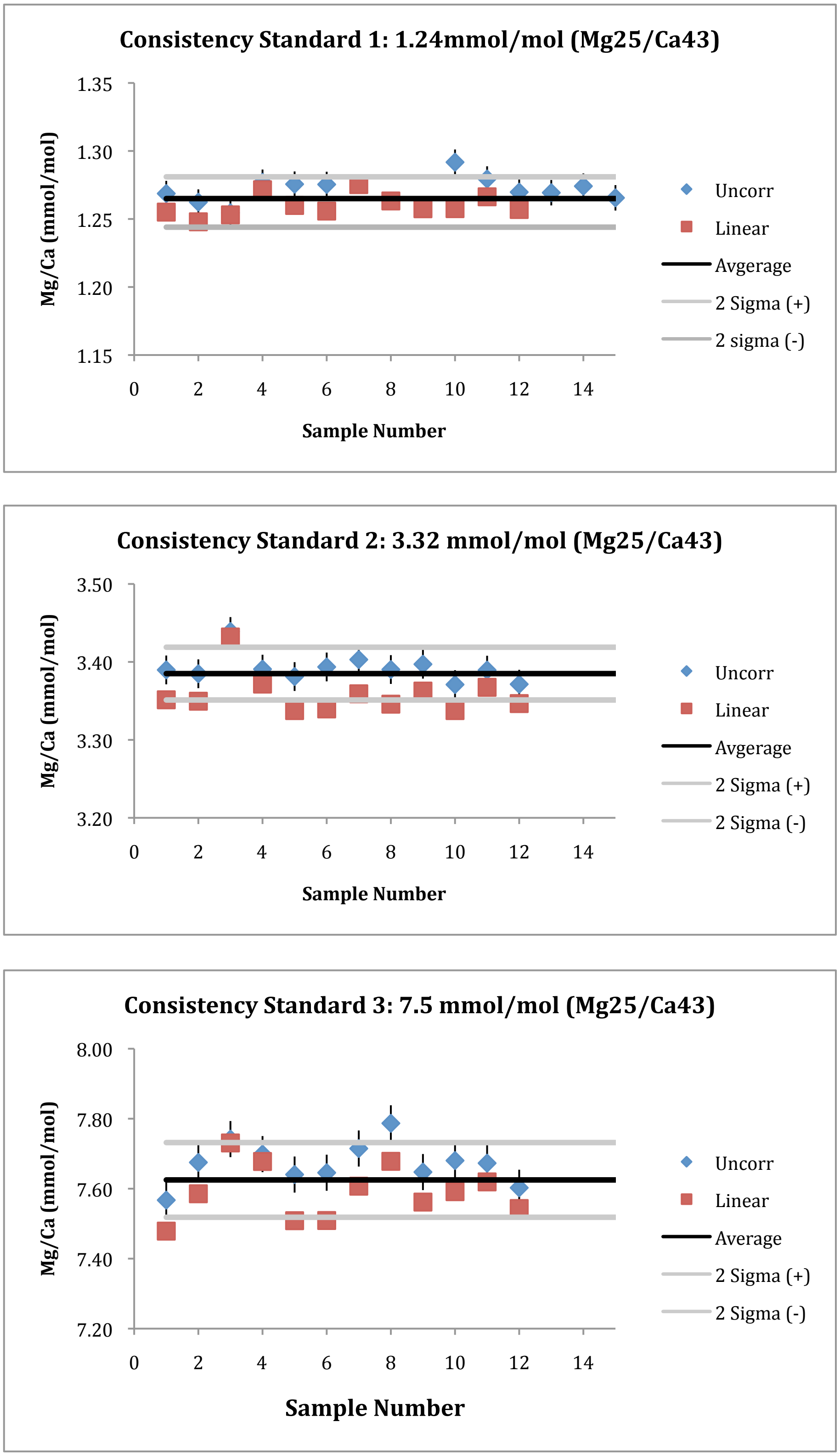

Figure Apx 2. Replicate Analysis of CSTD. Shown above are the three consistency standard solutions(CSTD) which are measured for every run. Long term analytical precision of the consistency standards with CS1, CS2 and CS3 were ±0.62%, ±0.50% and ±0.70 % respectively.

Table Apx6. Consistency Standards: The statistics for the data shown in Figure 2**.**

Standard	Statistics	Mg^{25}/Ca^{43} Sr^{86++} Corr'ed	Mg^{25}/Ca^{43} Linear Matrix Corr'ed
CSTD 1	Average	1.272	1.260
	Standard Dev.	0.009	0.008
	%RSD	0.7%	0.6%
CSTD 2	Average	3.392	3.358
	Standard Dev.	0.018	0.027
	%RSD	0.5%	0.8%
CSTD 3	Average	7.673	7.591
	Standard Dev.	0.052	0.072
	%RSD	0.7%	0.9%

Standard	Statistics	Sr^{86} or Sr^{88}/Ca^{43} Sr^{86++} Corr'ed	Sr^{86} or Sr^{88}/Ca^{43} Linear Matrix Corr'ed
CSTD 1	Average	0.458	0.450
	Standard Dev.	0.004	0.010
	%RSD	1.0%	2.3%
CSTD 2	Average	0.907	0.892
	Standard Dev.	0.009	0.020
	%RSD	1.0%	2.2%
CSTD 3	Average	1.807	1.775
	Standard Dev.	0.016	0.047
	%RSD	0.9%	2.7%

Raw Mg/Ca, $\delta^{18}O$ and $\delta^{13}C$ from all Cores:

Core: BJ8-03 7GGC

Depth (cm)	Age (CE)	δ18O (calcite)	δ13C (calcite)	Mg/Ca (mmol/mol)	SST (°C)	δ18O sw
4.5		-2.645	0.515	4.541	27.56	-0.07
5.5		-2.750	0.904	4.625	27.77	-0.13
10.5	1885.0	-2.982	0.572	4.638	27.80	-0.36
11.5	1871.0			4.712	27.97	
12.5	1857.0	-2.635	1.175	4.695	27.93	0.02
13.5	1843.0	-2.672	1.022	4.191	26.67	-0.28
14.5	1829.0	-2.834	0.947	4.273	26.89	-0.40
16.5	1801.0	-2.746	1.226	4.252	26.83	-0.32
17.5	1787.0	-2.710	0.854	4.415	27.25	-0.20
18.5	1773.0	-2.815	1.008	4.090	26.40	-0.48
19.5	1759.0	-2.623	0.778	4.210	26.72	-0.22

20.5	1745.0	-2.563	0.959	4.337	27.05	-0.09
21.5	1731.0			4.085	26.39	
22.5	1717.0	-2.525	1.431	4.046	26.28	-0.22
23.5	1700.5	-2.872	1.075	4.101	26.43	-0.53
24.5	1684.1	-2.646	0.796	4.213	26.73	-0.24
25.5	1667.6	-2.947	0.862	4.435	27.30	-0.43
26.5	1651.2	-2.975	1.269	4.425	27.28	-0.46
27.5	1634.7	-2.578	0.799	4.359	27.11	-0.10
28.5	1618.3	-2.979	0.981	4.239	26.80	-0.56
29.5	1601.8	-2.836	1.157	3.947	26.01	-0.59
30.5	1585.4	-2.849	0.748	4.122	26.49	-0.50
31.5	1568.9			4.325	27.02	
32.5	1552.4	-2.918	1.082	4.196	26.69	-0.53
33.5	1536.0	-2.621	0.908	4.584	27.67	-0.02
34.5	1519.5	-3.004	0.794	4.310	26.98	-0.55
35.5	1503.1	-2.868	0.927	4.317	27.00	-0.41
36.5	1486.6	-3.109	0.905	3.932	25.96	-0.87
37.5	1470.2	-2.802	1.104	4.125	26.50	-0.45
38.5	1453.7	-2.781	0.869	4.153	26.57	-0.41
40.0	1429.0	-2.670	0.455	4.176	26.63	-0.29
41.5	1404.3	-2.659	1.184	4.164	26.60	-0.28
42.5	1387.9	-2.437	0.695	4.617	27.75	0.18
43.5	1371.4	-2.956	0.678	4.298	26.95	-0.51
44.5	1355.0	-2.624	1.187	5.037	28.72	0.19
45.5	1338.5	-2.928	0.950	4.129	26.51	-0.57
46.5	1322.1	-2.619	0.546	4.360	27.11	-0.14
47.5	1305.6	-2.770	0.584	4.224	26.76	-0.36
48.5	1289.1	-2.846	1.116	4.123	26.49	-0.49
50.0	1264.5	-2.684	0.988	4.370	27.14	-0.20
51.5	1244.0	-2.712	0.960	4.404	27.22	-0.21
52.5	1235.9	-2.899	0.777	4.349	27.08	-0.42
53.5	1227.9	-2.705	1.067	4.448	27.33	-0.18
54.5	1219.9	-2.704	0.921	4.399	27.21	-0.20
55.5	1211.8	-2.628	0.929	4.133	26.52	-0.27
56.5	1203.8	-2.578	0.887	4.163	26.60	-0.20
57.5	1195.7	-2.999	0.793	4.669	27.87	-0.36
58.5	1187.7	-2.808	1.280	4.323	27.02	-0.35
59.5	1179.6	-2.668	1.053	4.296	26.95	-0.22
60.5	1171.6	-2.635	0.765			
61.5	1163.5	-2.796	0.529	4.580	27.66	-0.20
62.5	1155.5	-2.895	0.585	4.592	27.69	-0.29
63.5	1147.5	-2.604	0.814	4.437	27.31	-0.08
64.5	1139.4	-2.609	0.917	4.462	27.37	-0.07
65.5	1131.4	-2.760	0.754	4.645	27.82	-0.13
66.5	1123.3	-2.691	1.049	4.680	27.90	-0.05
67.5	1115.3	-2.638	0.823	4.456	27.35	-0.11
68.5	1107.2	-2.882	1.294	4.327	27.03	-0.42

69.5	1099.2	-2.877	0.666	4.389	27.19	-0.38
70.5	1091.1	-2.912	1.087	4.601	27.71	-0.31
71.5	1083.1	-2.810	1.176	4.497	27.46	-0.26
72.5	1075.1	-2.629	1.020	4.459	27.36	-0.10
73.5	1067.0	-2.776	1.202	4.663	27.86	-0.14
74.5	1059.0	-2.572	1.054	4.621	27.76	0.04
75.5	1050.9	-2.550	1.070	4.603	27.71	0.06
76.5	1042.9	-2.715	1.059	4.216	26.74	-0.31
77.5	1034.8	-2.635	0.771	4.370	27.14	-0.15
78.5	1026.8	-2.821	1.107	4.427	27.28	-0.30
79.5	1018.7	-2.800	0.993	4.719	27.99	-0.14
80.5	1010.7	-2.814	0.835	4.510	27.49	-0.26
81.5	1002.7	-2.760	0.676	4.712	27.97	-0.10
82.5	994.6	-2.850	0.853	4.386	27.18	-0.36
83.5	986.6	-2.695	0.995	4.317	27.00	-0.24
84.5	978.5	-2.653	0.922	4.547	27.58	-0.08
85.5	970.5	-2.680	0.900	4.479	27.41	-0.14
86.5	962.4	-2.625	0.797	4.424	27.27	-0.11
87.5	954.4	-2.759	0.941	4.575	27.65	-0.17
88.5	946.3	-2.778	0.710	4.506	27.48	-0.22
89.5	938.3	-2.728	0.894			
90.5	930.3	-2.620	1.008	4.549	27.58	-0.04
91.5	922.2	-2.843	0.619	4.660	27.85	-0.21
92.5	914.2	-2.746	1.024	4.727	28.01	-0.08
93.5	906.1	-2.797	0.887	4.470	27.39	-0.26
94.5	898.1	-2.696	0.892	4.267	26.87	-0.27
95.5	890.0	-2.496	0.919	4.621	27.76	0.12
96.5	882.0			4.361	27.11	
97.5	873.9	-2.549	1.221	4.443	27.32	-0.02
98.5	865.9	-2.686	1.208	4.418	27.26	-0.17
99.5	857.9	-2.753	1.097	4.672	27.88	-0.11
103.5	825.7	-2.413	0.908	4.580	27.66	0.18
107.5	793.5	-2.550	0.984	4.841	28.28	0.17
111.5	761.3	-2.692	0.846	4.799	28.18	0.01
115.5	729.2	-2.567	1.069	4.562	27.62	0.02
119.5	697.0	-2.773	1.184	5.062	28.77	0.05
123.5	664.8	-2.612	1.298	4.580	27.66	-0.02
127.5	632.6	-2.723	1.300	4.508	27.48	-0.16
131.5	600.4	-2.562	0.963	4.427	27.28	-0.05
135.5	568.3	-2.598	1.015	4.784	28.14	0.10
139.5	536.1	-2.584	0.932	4.641	27.81	0.04
143.5	503.9	-2.445	1.118	4.965	28.56	0.34
147.5	471.7	-2.671	1.193	4.560	27.61	-0.09
151.5	439.6	-2.763	0.976	4.855	28.31	-0.03
155.5	407.4	-3.051	1.069	5.212	29.09	-0.16
159.5	375.2	-2.652	0.899	4.908	28.43	0.10
163.5	343.0	-2.573	0.933	5.021	28.68	0.23

164.5	329.9	-2.782	0.995	5.041	28.72	0.03
165.5	311.8	-3.138	1.234	5.050	28.74	-0.32
166.5	293.6	-2.959	1.048	4.651	27.83	-0.33
167.5	275.5	-2.618	1.051			
168.5	257.3	-2.637	0.950	4.457	27.36	-0.11
169.5	239.2			4.954	28.53	
170.5	221.1			5.270	29.22	
172.5	184.8	-3.026	1.068	4.661	27.85	-0.39
173.5	166.6			4.788	28.15	
174.5	148.5	-3.094	1.151	4.632	27.78	-0.47
175.5	130.3			4.458	27.36	
176.5	112.2	-2.857	0.958	4.587	27.68	-0.26
177.5	94.0	-2.936	1.033	4.482	27.42	-0.39

Core: BJ8-03 85GGC

Depth (cm)	Age (CE)	d18O (calcite)	d13C (calcite)	Mg/Ca (mmol/mol)	SST (°C)	d18O sw
0.5		-3.189	0.95	5.028	28.70	-0.38
4	1991.2			4.901	28.41	
6	1967.0	-2.938	0.79	5.357	29.40	0.02
8	1942.8	-3.154	0.97	4.645	27.82	-0.53
10	1918.6	-2.985	1.01	5.082	28.81	-0.15
12	1894.3	-3.169	0.56	5.688	30.07	-0.07
14	1870.1	-2.953	1.08	4.879	28.36	-0.21
16	1845.9	-3.004	1.02	4.811	28.20	-0.30
18	1821.7	-3.007	1.13	5.111	28.88	-0.16
20	1797.4			4.923	28.46	
22	1773.2	-2.975	0.71	4.759	28.08	-0.29
24	1749.0	-3.079	1.13	5.145	28.95	-0.22
26	1724.8	-3.068	1.06	4.808	28.20	-0.36
28	1700.6	-3.050	0.59	4.714	27.98	-0.39
30	1676.3	-2.951	1.03	4.913	28.44	-0.19
32	1652.1	-3.057	1.09	4.796	28.17	-0.36
34	1627.9	-3.178	0.90	4.919	28.45	-0.42
36	1603.7	-2.890	0.88	5.674	30.04	0.20
38	1579.4	-2.870	0.89	4.566	27.63	-0.28
40	1555.2	-3.024	0.97	4.748	28.06	-0.35
42	1531.0	-2.988	1.07	4.978	28.58	-0.20
44	1506.8	-3.191	1.11	4.593	27.69	-0.59
45	1494.7	-2.989	1.01	5.231	29.13	-0.09
48	1458.3	-2.964	0.99	4.873	28.35	-0.23
50	1434.1	-2.947	1.10	4.449	27.34	-0.42
52	1411.0	-3.030	1.28	4.679	27.90	-0.39
54	1389.1	-3.049	1.14	5.041	28.72	-0.23
56	1367.2	-2.950	1.04	5.276	29.23	-0.03

58	1345.3	-3.094	1.06	4.728	28.01	-0.43
60	1323.4	-3.102	1.09	5.022	28.68	-0.29
62	1301.4	-3.032	1.18	4.941	28.50	-0.26
64	1279.5	-3.141	1.05	5.520	29.73	-0.11
66	1257.6	-2.989	1.14	4.651	27.83	-0.36
68	1235.7	-3.096	1.09	4.673	27.88	-0.45
70	1213.8	-2.950	1.02	4.692	27.93	-0.30
72	1191.8	-3.079	0.90	5.165	28.99	-0.21
74	1169.9	-3.078	1.06	4.380	27.16	-0.59
76	1148.0	-2.918	1.09	4.992	28.62	-0.12
78	1126.1	-3.148	1.22	4.766	28.10	-0.46
80	1104.2	-3.075	1.25	5.241	29.16	-0.17
82	1082.2	-3.023	1.09	4.643	27.81	-0.40
84	1060.3	-3.185	0.92	4.910	28.43	-0.43
86	1038.4	-3.101	1.11	4.841	28.28	-0.38
88	1016.5	-3.110	1.01	5.024	28.69	-0.30
90	994.6	-3.040	0.98	4.905	28.42	-0.29
92	972.6	-2.958	1.11	4.926	28.47	-0.19
94	950.7	-3.166	1.14	4.695	27.93	-0.51
96	928.8	-3.081	1.08	5.670	30.03	0.01
98	906.9	-2.908	1.13	4.791	28.16	-0.21
100	885.0	-3.078	0.85	5.005	28.64	-0.28
102	857.5	-3.160	1.23	5.219	29.11	-0.26
104	824.4	-2.916	0.94	5.985	30.63	0.30
108	758.2	-2.966	0.84	5.238	29.15	-0.06
112	692.0	-3.107	1.04	5.126	28.91	-0.25
116	625.8	-2.973	1.10	5.154	28.97	-0.11
118	592.7	-2.935	1.36	5.032	28.70	-0.12
124	493.4	-3.159	1.13	5.986	30.63	0.06
128	427.2	-2.928	0.99	4.905	28.42	-0.17
132	361.0	-3.130	0.90	4.764	28.10	-0.44
136	294.8	-3.101	0.99	5.242	29.16	-0.19
140	228.6	-3.083	0.99	5.092	28.84	-0.24
144	162.4	-3.157	0.93	4.906	28.42	-0.40
148	96.2	-2.974	0.75	4.780	28.13	-0.28
152	30.0	-2.981	0.73	5.300	29.28	-0.05
156	-36.2	-3.308	0.95	4.917	28.45	-0.55
160	-102.4	-3.158	1.03	5.387	29.46	-0.19
164	-168.6	-3.198	0.97	5.115	28.89	-0.35
168	-234.8	-2.980	0.98	5.861	30.40	0.19
172	-301.0	-2.913	1.12	5.610	29.91	0.15
176	-358.9	-3.022	0.89	5.043	28.73	-0.20
180	-416.7	-2.954	0.85	6.258	31.13	0.36
184	-474.6	-3.212	1.09	4.921	28.46	-0.45
188	-532.5	-3.007	0.97	5.115	28.89	-0.16
192	-590.3	-2.972	0.94	5.267	29.21	-0.05

196	-648.2	-2.881	0.82	5.157	28.98	-0.01
200	-706.0	-3.040	0.80	5.296	29.27	-0.11
204	-763.9	-3.080	0.99	4.688	27.92	-0.43
208	-821.8			4.669	27.87	
216	-937.5			5.167	29.00	

BJ8-03 6MC

Depth (cm)	Age (CE)	δ18O (calcite)	δ13C (calcite)	Mg/Ca (mmol/mol)	SST (°C)	δ18O sw
0.25	2000.6			4.790	28.16	
0.75	1993.6			4.902	28.41	
2.5	1986.6	-2.784	0.552	4.838	28.27	-0.06
3.5	1979.1	-2.958	0.368	4.818	28.22	-0.25
4.5	1971.7	-2.805	0.780	5.133	28.93	0.05
5.5	1964.2	-2.547	0.719	4.498	27.46	0.01
6.5	1956.8	-2.838	0.727	4.777	28.13	-0.15
7.5	1949.3	-2.804	0.807	4.682	27.90	-0.16
8.5	1941.8	-2.551	0.664	4.614	27.74	0.06
9.5	1934.4	-2.765	0.788	4.669	27.87	-0.13
10.5	1926.9	-3.006	0.616	4.562	27.61	-0.42
11.5	1919.5	-2.564	1.294	4.670	27.87	0.08
12.5	1912.0	-2.63	1.007	4.542	27.57	-0.05
13.5	1904.5	-2.731	0.810	4.516	27.50	-0.17
14.5	1897.1	-2.757	0.603	4.423	27.27	-0.24
15.5	1889.6	-2.596	0.756	4.603	27.72	0.01
16.5	1882.2	-2.692	0.868	4.567	27.63	-0.10
17.5	1874.7	-2.695	0.928	4.317	27.00	-0.24
18.5	1868.0	-2.648	1.046			
19.5	1859.8	-2.863	1.075	4.302	26.96	-0.41
20.5	1852.3	-2.681	0.958	4.179	26.64	-0.30
21.5	1844.8	-2.824	0.912	4.354	27.10	-0.35
22.5	1837.4	-2.932	0.878	4.457	27.36	-0.40
23.5	1829.9	-2.836	0.914	4.611	27.73	-0.23
24.5	1822.5	-2.597	0.829	4.379	27.16	-0.11
25.5	1815.0	-2.428	1.102	4.301	26.96	0.02
26.5	1807.5	-2.821	1.190	4.266	26.87	-0.39
27.5	1800.0	-2.712	1.060	4.591	27.68	-0.11
28.5	1792.5	-2.611	1.023	4.403	27.22	-0.11
29.5	1785.0	-2.627	0.927	4.353	27.09	-0.15
30.5	1777.5	-3.038	1.351	4.002	26.16	-0.76

31.5	1770.0	-2.689	1.053	4.339	27.06	-0.22
32.5	1762.5	-2.578	1.315	4.561	27.61	0.01
33.5	1755.0	-2.629	1.032	4.349	27.08	-0.15
34.5	1747.5	-2.738	1.071	4.173	26.63	-0.36
35.5	1740.0	-2.742	1.107	4.145	26.55	-0.38
36.5	1732.5	-2.787	1.099	4.294	26.94	-0.34
37.5	1725.0	-2.637	0.974	4.001	26.16	-0.36
38.5	1717.5	-2.574	1.260	4.177	26.64	-0.19
39.5	1710.0	-2.784	1.304	4.033	26.25	-0.48
40.5	1702.5	-2.689	1.303	4.277	26.90	-0.25
41.5	1695.0	-2.701	1.440	4.191	26.67	-0.31
42.5	1687.5	-3.017	1.232	4.111	26.46	-0.67
43.5	1680.0	-2.729	1.238	4.372	27.14	-0.24
44.5	1673.8	-2.581	1.294	4.063	26.33	-0.26
45.5	1667.6	-2.749	1.362	4.255	26.84	-0.32
46.5	1661.4	-2.528	1.066	4.479	27.41	0.02

BJ8-03 84MC

Depth (cm)	Age (CE)	δ18O (calcite)	δ13C (calcite)	Mg/Ca (mmol/mol)	SST (^{o}C)	δ18O sw
2.50	1986.0	-3.117	0.719	5.062	28.77	-0.29
3.50	1982.0	-3.301	0.588	5.163	28.99	-0.43
4.50	1977.0	-3.271	0.586	4.757	28.08	-0.59
5.50	1968.5	-3.160	0.836	5.159	28.98	-0.29
6.50	1963.9	-3.007	0.699	4.946	28.51	-0.23
7.50	1959.4	-3.134	0.995	5.205	29.08	-0.24
8.50	1951.6	-3.178	0.855	4.652	27.83	-0.55
9.50	1943.8	-3.085	0.982	4.853	28.30	-0.36
10.50	1936.0	-3.280	0.920	5.103	28.86	-0.43
11.50	1928.2	-3.142	1.216	4.906	28.42	-0.39
12.50	1920.4	-3.108	0.819	4.767	28.10	-0.42
13.50	1912.6	-3.210	0.878	5.230	29.13	-0.31
14.50	1904.8	-3.222	0.997	4.807	28.20	-0.52
15.50	1897.0	-3.176	0.950			
16.50	1889.2	-3.206	1.012	4.693	27.93	-0.55
17.50	1881.4	-3.130	1.143	4.759	28.08	-0.45
18.50	1873.6	-3.057	1.053	4.707	27.96	-0.40
19.50	1865.8	-3.202	1.005	4.806	28.19	-0.50
20.50	1858.0	-3.167	1.054	4.878	28.36	-0.43
21.50	1850.2	-3.147	1.084	4.790	28.16	-0.45
22.50	1842.4	-3.059	1.016	4.944	28.51	-0.29
23.50	1834.6	-2.975	1.072	4.853	28.30	-0.25
24.50	1826.8	-3.082	1.007	4.893	28.39	-0.33
25.50	1819.0	-3.046	1.102	4.926	28.47	-0.28
26.50	1811.2	-3.144	1.131	4.889	28.38	-0.40

27.50	1803.4	-3.147	1.045	4.992	28.62	-0.35
28.50	1795.6	-3.070	1.072	4.971	28.57	-0.29
29.50	1787.8	-3.068	1.163	4.974	28.58	-0.28
30.50	1780.0	-3.044	1.028	5.114	28.88	-0.19
31.50	1772.2	-3.238	1.111	4.944	28.51	-0.47
32.50	1764.4	-3.090	1.084	4.735	28.03	-0.42
33.50	1756.6	-2.947	1.225	4.597	27.70	-0.34
34.50	1748.8	-3.025	1.034	5.532	29.76	0.01
35.50	1741.0	-3.252	1.046	5.233	29.14	-0.35
36.50	1733.2	-3.135	1.099	5.490	29.67	-0.12
37.50	1725.4	-3.035	1.175	4.891	28.39	-0.29
38.50	1717.6	-3.231	1.042	4.460	27.36	-0.70

BJ8-03 142MC

Depth (cm)	**Age (CE)**	**δ18O (calcite)**	**δ13C (calcite)**	**Mg/Ca (mmol/mol)**	**SST (°C)**	**δ18O sw**
0.5	2004.0			4.797	28.17	
2.0	2003.0	-3.192	0.746	4.904	28.42	-0.44
3.5	2002.0	-3.313	1.045	5.055	28.76	-0.49
4.5	2001.0	-3.245	0.962	4.788	28.15	-0.55
5.5	2000.0	-3.187	0.899	5.021	28.68	-0.38
6.5	1995.4	-3.315	1.027	4.884	28.37	-0.57
7.5	1990.5	-3.311	0.797	4.718	27.99	-0.65
8.5	1985.7	-3.25	0.972	4.822	28.23	-0.54
9.5	1980.8	-3.181	0.930	4.748	28.06	-0.50
10.5	1975.9	-3.089	0.895	4.753	28.07	-0.41
11.5	1971.8	-3.449	0.724	4.980	28.59	-0.66
12.5	1968.5	-3.202	0.812	4.712	27.97	-0.54
13.5	1965.1	-3.285	1.095	4.720	27.99	-0.62
14.5	1961.8	-3.394	0.993	4.784	28.14	-0.70
15.5	1958.5	-3.469	0.902	4.538	27.56	-0.90
16.5	1955.1	-3.262	0.950	5.023	28.68	-0.45
17.5	1951.8	-3.127	0.705	4.948	28.52	-0.35
18.5	1948.4	-3.126	0.915	4.503	27.47	-0.57
19.5	1945.1	-3.372	0.898	4.834	28.26	-0.65
20.5	1941.7	-3.189	1.039	4.653	27.83	-0.56
21.5	1938.4	-3.277	1.083	4.717	27.99	-0.61
22.5	1935.1	-3.404	1.061	4.602	27.71	-0.80
23.5	1931.7	-3.283	1.124	4.549	27.58	-0.70
24.5	1928.4			4.645	27.81	
25.5	1925.0	-3.299	1.225	4.419	27.26	-0.79
26.5	1921.7	-3.088	0.793	4.588	27.68	-0.49
27.5	1918.3	-3.332	1.092	4.407	27.23	-0.83
28.5	1915.0	-3.321	0.876	4.375	27.15	-0.83
29.5	1909.6	-3.487	0.801	4.494	27.45	-0.94
30.5	1904.2	-3.121	1.033	4.817	28.22	-0.41
31.5	1898.8	-3.423	0.975	4.889	28.39	-0.68

32.5	1893.4	-3.42	0.875	4.761	28.09	-0.74
33.5	1888.0	-3.321	1.149	5.362	29.41	-0.36
34.5	1882.6	-3.075	1.166			
35.5	1877.2	-2.881	1.166			
36.5	1871.8	-3.209	0.952			
37.5	1866.4	-2.926	0.957	4.436	27.30	-0.40
38.5	1861.0	-3.083	0.875	4.714	27.98	-0.42
39.5	1855.6					
40.5	1850.2	-3.351	0.985			
43.5	1833.9			4.731	28.02	
44.5	1828.5					
45.5	1823.1	-3.117	1.154	5.021	28.68	-0.31
46.5	1817.7	-3.082	1.049			

Raw Al/Ca, Fe/Ca and Mn/Ca Data for all cores:

Core: BJ8-03 7GGC

Depth (cm)	Age (CE)	R Ca	Al/Ca (μmol/mol)	Fe/Ca (μmol/mol)	Mn/Ca (μmol/mol)	Rejected
4.5		0.352	567	169	45.4	
5.5		0.547	150	49	40.5	
10.5	1885.0	0.252	110	41	49.6	
11.5	1871.0	0.408	191	51	32.4	
12.5	1857.0	0.623	1859	508	56.8	
13.5	1843.0	0.456	153	23	47.2	
14.5	1829.0	0.352	325	39	37.6	
16.5	1801.0	0.400	148	114	64.6	
17.5	1787.0	0.656	440	38	59.5	
18.5	1773.0	0.621	168	46	44.4	
19.5	1759.0	0.316	164	58	44.3	
20.5	1745.0	0.401	513	41	44.9	
21.5	1731.0	0.325	124	69	64.2	
22.5	1717.0	0.282	96	19	57.6	
23.5	1700.5	0.445	1538	57	49.3	
24.5	1684.1	0.459	66	48	113.5	
25.5	1667.6	0.483	437	240	70.7	
26.5	1651.2	0.450	54	92	38.8	
27.5	1634.7	0.384	89	42	39.2	
28.5	1618.3	0.284	48	23	50.8	
29.5	1601.8	0.338	42	21	44.4	
30.5	1585.4	0.371	169	133	203.0	
31.5	1568.9	0.650	50	211	170.0	
32.5	1552.4	0.400	141	123	140.4	
33.5	1536.0	0.615	59	70	175.5	
34.5	1519.5	0.431	1304	400	60.9	
35.5	1503.1	0.374	162	50	49.1	
36.5	1486.6	0.391	113	18	63.1	

37.5	1470.2	0.643	107	160	63.8	
38.5	1453.7	0.355	323	45	63.7	
40.0	1429.0	0.722	114	61	158.9	
41.5	1404.3	0.322	83	117	57.2	
42.5	1387.9	0.450	2533	51	65.6	R
43.5	1371.4	0.357	170	26	67.9	
44.5	1355.0	0.399	353	181	119.1	
45.5	1338.5	0.446	97	76	60.0	
46.5	1322.1	0.516	101	73	158.1	
47.5	1305.6	0.364	200	24	50.1	
48.5	1289.1	0.234	202	31	46.3	
50.0	1264.5	0.956	162	69	150.5	
51.5	1244.0	0.236	210	20	65.9	
52.5	1235.9	0.393	305	148	54.4	
53.5	1227.9	0.672	147	81	100.0	
54.5	1219.9	0.592	105	76	212.4	
55.5	1211.8	0.751	504	75	69.4	
56.5	1203.8	0.297	114	17	83.9	
57.5	1195.7	0.266	695	59	151.6	
58.5	1187.7	0.462	207	34	84.3	
59.5	1179.6	0.949	71	41	111.1	
60.5	1171.6	0.059	556	1311	110.8	R
61.5	1163.5	1.201	87	66	144.3	
62.5	1155.5	0.993	237	343	134.9	
63.5	1147.5	0.854	270	40	123.9	
64.5	1139.4	1.010	55	202	128.3	
65.5	1131.4	1.183	95	148	99.2	
66.5	1123.3	0.852	173	25	106.5	
67.5	1115.3	0.720	69	26	102.7	
68.5	1107.2	0.522	232	130	71.1	
69.5	1099.2	0.549	276	133	69.7	
70.5	1091.1	0.832	91	56	121.9	
71.5	1083.1	1.072	67	81	119.2	
72.5	1075.1	1.064	105	109	93.9	
73.5	1067.0	0.820	51	87	77.8	
74.5	1059.0	0.957	119	257	82.7	
75.5	1050.9	1.091	63	105	80.9	
76.5	1042.9	0.935	98	336	71.6	
77.5	1034.8	0.957	215	100	75.0	
78.5	1026.8	0.928	47	70	83.8	
79.5	1018.7	0.757	116	43	75.4	
80.5	1010.7	0.788	63	62	77.5	
81.5	1002.7	0.772	125	97	83.0	
82.5	994.6	0.821	240	380	90.4	
83.5	986.6	0.653	116	63	84.6	
84.5	978.5	0.510	280	170	64.7	
85.5	970.5	0.710	194	220	80.6	

86.5	962.4	0.739	121	72	99.8	
87.5	954.4	0.182	430	332	79.6	
88.5	946.3	0.569	78	347	86.4	
89.5	938.3					
90.5	930.3	0.678	227	263	72.6	
91.5	922.2	0.615	273	278	72.6	
92.5	914.2	0.711	121	98	76.1	
93.5	906.1	0.491	145	207	91.6	
94.5	898.1	0.639	184	75	93.6	
95.5	890.0	0.168	1120	57	62.5	
96.5	882.0	0.417	135	141	79.6	
97.5	873.9	0.408	174	232	77.1	
98.5	865.9	0.537	287	145	82.3	
99.5	857.9	1.006	149	275	100.7	
103.5	825.7	0.931	304	0	88.5	
107.5	793.5	0.886	415	0	103.4	
111.5	761.3	0.577	453	0	81.4	
115.5	729.2	0.829	309	189	91.2	
119.5	697.0	0.759	462	0	97.5	
123.5	664.8	0.670	326	701	110.3	
127.5	632.6	0.431	133	78	77.6	
131.5	600.4	0.949	840	93	88.7	
135.5	568.3	1.037	186	349	89.5	
139.5	536.1	0.774	196	605	101.4	
143.5	503.9	0.902	384	0	98.5	
147.5	471.7	0.934	340	0	91.3	
151.5	439.6	0.671	395	699	103.4	
155.5	407.4	0.983	602	0	116.5	
159.5	375.2	0.917	719	367	103.9	
163.5	343.0	0.773	578	0	109.3	
164.5	329.9	0.815	796	0	126.8	
165.5	311.8	0.696	663	0	101.7	
166.5	293.6	0.668	543	391	104.1	
168.5	275.5	0.438	363	359	75.1	
169.5	257.3	1.296	503	0	107.8	
170.5	239.2	0.774	852	0	100.3	
171.5	221.1	0.814	949	0	112.5	
172.5	184.8	1.004	298	277	123.2	
173.5	166.6	1.063	529	536	109.2	
174.5	148.5	0.710	579	293	96.7	
175.5	130.3	0.566	446	126	93.4	
176.5	112.2	0.815	279	184	83.2	
177.5	94.0	0.310	364	655	65.9	

Core: BJ8-03 85GGC

Depth (cm)	Age (CE)	R Ca	Al/Ca (μmol/mol)	Fe/Ca (μmol/mol)	Mn/Ca (μmol/mol)	Rejected
0.5		0.726	620	5283	49.1	R
4	1991.2	0.665	243	13344	45.5	R
6	1967.0	0.347	684	244	43.3	
8	1942.8	0.892	781	160	55.5	
10	1918.6	0.424	277	426	33.7	
12	1894.3	0.733	807	95	45.9	
14	1870.1	0.469	2127	300	35.7	R
16	1845.9	0.691	631	359	59.7	
18	1821.7	0.447	487	216	42.7	
20	1797.4	0.561	491	252	51.7	
22	1773.2	0.222	217	880	34.7	
24	1749.0	0.719	163	264	72.1	
26	1724.8	0.237	355	823	51.0	
28	1700.6	0.748	1891	779	55.8	
30	1676.3	0.694	223	499	41.0	
32	1652.1	0.990	316	113	60.5	
34	1627.9	0.309	296	381	44.5	
36	1603.7	0.307	1487	336	66.1	
38	1579.4	0.675	129	224	37.3	
40	1555.2	0.983	101	85	66.1	
42	1531.0	0.460	490	1751	44.9	
44	1506.8	0.448	578	855	41.9	
45	1494.7	0.275	2066	525	48.2	R
48	1458.3	0.886	230	202	66.9	
50	1434.1	0.684	540	264	45.8	
52	1411.0	0.573	239	488	49.1	
54	1389.1	0.183	754	876	44.3	
56	1367.2	1.112	476	309	80.0	
58	1345.3	0.587	78	178	46.1	
60	1323.4	0.775	203	122	41.9	
62	1301.4	0.718	527	403	47.0	
64	1279.5	0.809	268	255	62.8	
66	1257.6	0.641	135	349	41.0	
68	1235.7	0.743	278	328	47.9	
70	1213.8	0.452	384	751	40.6	
72	1191.8	0.651	2192	324	58.2	R
74	1169.9	0.334	67	445	29.9	
76	1148.0	0.429	1021	221	49.4	
78	1126.1	0.672	127	295	40.3	
80	1104.2	0.553	289	317	65.6	
82	1082.2	0.313	129	1537	34.2	
84	1060.3	1.048	314	216	44.2	
86	1038.4	0.314	445	885	44.3	

88	1016.5	0.977	566	160	58.8	
90	994.6	0.545	326	228	44.5	
92	972.6	0.867	246	223	47.4	
94	950.7	0.373	144	365	42.5	
96	928.8	0.951	309	204	68.4	
98	906.9	0.455	101	223	43.8	
100	885.0	0.718	1795	386	44.0	
102	857.5	0.538	414	241	41.4	
104	824.4	0.795	812	268	64.9	
108	758.2	0.876	379	312	43.7	
112	692.0	0.971	319	175	56.1	
116	625.8	1.115	628	145	42.3	
118	592.7	1.367	204	142	44.1	
124	493.4	0.657	908	236	47.7	
128	427.2	0.898	463	306	46.8	
132	361.0	0.836	159	146	34.6	
136	294.8	0.795	547	149	50.3	
140	228.6	0.703	445	53	45.3	
144	162.4	0.945	95	50	48.1	
148	96.2	0.882	171	70	43.5	
152	30.0	0.749	290	36	52.1	
156	-36.2	0.589	144	127	53.8	
160	-102.4	1.152	417	31	72.1	
164	-168.6	0.625	267	27	34.4	
168	-234.8	0.533	807	97	63.2	
172	-301.0	0.775	584	31	52.4	
176	-358.9	0.666	257	25	41.0	
180	-416.7	0.748	1344	44	43.0	
184	-474.6	1.144	198	36	49.7	
188	-532.5	0.607	378	163	38.9	
192	-590.3	1.092	318	33	43.2	
196	-648.2	0.911	349	55	46.8	
200	-706.0	1.064	305	71	53.9	
204	-763.9	0.530	118	49	32.9	
208	-821.8	1.026	28	10	41.9	
216	-937.5	1.018	191	26	53.1	

Core: BJ8-03 6MC

Depth (cm)	Age (CE)	R Ca	Al/Ca (μmol/mol)	Fe/Ca (μmol/mol)	Mn/Ca (μmol/mol)	Rejected
0.25	2000.6	0.587	187	Error in Run	12.4	
0.75	1993.6	0.597	156	with Fe Data	30.2	
2.5	1986.6	0.992	147		64.9	
3.5	1979.1	0.680	58		37.3	
4.5	1971.7	0.799	316		46.6	
5.5	1964.2	1.045	203		54.2	
6.5	1956.8	1.058	115		61.3	
7.5	1949.3	0.893	241		43.7	
8.5	1941.8	0.594	79		40.8	
9.5	1934.4	1.087	190		68.2	
10.5	1926.9	0.829	60		61.2	
11.5	1919.5	1.191	433		63.6	
12.5	1912.0	1.089	109		53.5	
13.5	1904.5	1.057	121		43.7	
14.5	1897.1	0.736	88		53.6	
15.5	1889.6	1.026	121		58.9	
16.5	1882.2	0.914	90		56.4	
17.5	1874.7	1.040	81		56.9	
19.5	1859.8	0.809	55		39.2	
20.5	1852.3	0.576	390		27.8	
21.5	1844.8	1.064	377		53.7	
22.5	1837.4	0.396	167		52.9	
23.5	1829.9	0.821	220		49.1	
24.5	1822.5	1.043	124		63.7	
25.5	1815.0	1.046	276		40.8	
26.5	1807.5	0.956	812		50.4	
27.5	1800.0	0.971	151		61.6	
28.5	1792.5	1.050	73		59.6	
29.5	1785.0	0.810	160		61.6	
30.5	1777.5	0.691	103		48.4	
31.5	1770.0	0.602	78		62.3	
32.5	1762.5	0.931	120		74.4	
33.5	1755.0	1.088	146		76.2	
34.5	1747.5	1.023	796		61.5	
35.5	1740.0	1.159	152		84.4	
36.5	1732.5	1.028	60		68.4	
37.5	1725.0	0.791	32		63.0	
38.5	1717.5	1.000	106		81.6	
39.5	1710.0	0.625	39		73.9	
40.5	1702.5	1.010	102		81.3	
41.5	1695.0	0.747	54		69.7	
42.5	1687.5	0.780	35		67.8	
43.5	1680.0	1.403	247		77.2	
44.5	1673.8	1.018	35		68.5	

45.5	1667.6	1.092	206		79.8	
46.5	1661.4	0.763	43		50.1	

Core: BJ8-03 84MC

Depth (cm)	Age (CE)	R Ca	Al/Ca (μmol/mol)	Fe/Ca (μmol/mol)	Mn/Ca (μmol/mol)	Rejected
2.5	1986.0	0.602	232	182	19.3	
3.5	1982.0	0.487	168	199	19.0	
4.5	1977.0	0.719	395	68	32.3	
5.5	1968.5	0.777	212	86	29.2	
6.5	1963.9	0.775	196	102	28.9	
7.5	1959.4	0.688	320	65	30.5	
8.5	1951.6	0.773	107	81	20.7	
9.5	1943.8	0.847	163	44	24.3	
10.5	1936.0	1.013	79	36	27.6	
11.5	1928.2	0.890	79	61	27.2	
12.5	1920.4	1.215	67	107	42.1	
13.5	1912.6	0.940	438	57	48.1	
14.5	1904.8	0.497	70	167	29.6	
15.5	1897.0	0.001	25681	139051	166.9	R
16.5	1889.2	1.128	74	74	37.9	
17.5	1881.4	1.088	342	69	40.1	
18.5	1873.6	1.205	50	15	43.5	
19.5	1865.8	0.895	128	26	36.9	
20.5	1858.0	1.078	145	36	36.2	
21.5	1850.2	1.048	59	20	39.2	
22.5	1842.4	1.045	136	68	34.9	
23.5	1834.6	0.774	321	110	36.6	
24.5	1826.8	1.310	222	77	38.4	
25.5	1819.0	1.040	191	83	43.0	
26.5	1811.2	0.934	170	167	39.5	
27.5	1803.4	1.018	161	82	32.7	
28.5	1795.6	0.625	216	80	31.4	
29.5	1787.8	1.018	323	66	38.0	
30.5	1780.0	1.066	236	77	42.5	
31.5	1772.2	0.875	122	100	38.8	
32.5	1764.4	0.366	103	328	31.2	
33.5	1756.6	0.819	483	45	32.9	
34.5	1748.8	1.039	885	85	37.2	
35.5	1741.0	0.897	416	57	45.6	
36.5	1733.2	1.120	407	46	104.5	
37.5	1725.4	0.876	289	19	34.7	
38.5	1717.6	0.699	196	30	26.8	

Core: BJ8-03 142MC

Depth (cm)	Age (CE)	R Ca	Al/Ca (μmol/mol)	Fe/Ca (μmol/mol)	Mn/Ca (μmol/mol)	Rejected
0.5	2004.0	1.126	996	33	51.3	
2	2003.0	0.948	210	28	61.5	
3.5	2002.0	0.765	155	53	67.7	
4.5	2001.0	1.505	203	35	45.5	
5.5	2000.0	1.363	272	152	60.2	
6.5	1995.4	1.382	168	32	69.0	
7.5	1990.5	1.588	462	38	61.6	
8.5	1985.7	1.483	126	19	44.5	
9.5	1980.8	1.638	198	56	63.8	
10.5	1975.9	1.056	157	21	69.6	
11.5	1971.8	1.154	277	67	70.1	
12.5	1968.5	0.966	95	154	61.0	
13.5	1965.1	2.054	53	29	116.8	
14.5	1961.8	1.757	132	34	114.4	
15.5	1958.5	1.379	169	54	75.9	
16.5	1955.1	1.534	737	0	139.5	
17.5	1951.8	1.515	172	60	86.2	
18.5	1948.4	0.887	230	112	47.2	
19.5	1945.1	0.831	295	137	78.2	
20.5	1941.7	0.917	568	48	64.8	
21.5	1938.4	1.168	278	94	81.5	
22.5	1935.1	0.929	276	86	77.4	
23.5	1931.7	1.163	581	175	83.4	
24.5	1928.4	0.691	316	123	92.0	
25.5	1925.0	0.509	480	32	58.2	
26.5	1921.7	0.698	200	172	67.7	
27.5	1918.3	0.669	379	183	83.8	
28.5	1915.0	0.716	139	72	70.5	
29.5	1909.6	0.454	661	229	69.8	
30.5	1904.2	0.825	427	124	87.5	
31.5	1898.8	1.049	725	0	113.9	
32.5	1893.4	0.865	385	173	78.2	
33.5	1888.0	0.789	1142	0	83.3	
37.5	1866.4	0.552	356	496	56.6	
38.5	1861.0	0.427	289	227	67.7	
43.5	1833.9	0.599	219	83	71.3	
45.5	1823.1	0.380	455	210	350.0	R